JET PROPULSION LABORATORY

TECHNICAL MEMORANDUM 312-280

March 4, 1963

AUTHOR: M. Minovich

TITLE: The Determination, Analysis and Potentialities of Advanced Free-Fall Interplanetary Trajectories

DISTRIBUTION: Section 312 engineers, W.R. Hoover, F.H. Lesh, J.F. Scott, R.Y. Roth

SUMMARY:

When an interplanetary space vehicle approaches a planet on a free-fall trajectory the gravitational influence of the planet can radically change the vehicle's trajectory about the sun. It is possible for such vehicles to take advantage of this influence by passing the planet on a precisely calculated trajectory which will place the vehicle on an interceop trajectory with another planet. Of course these advanced trajectories taking a vehicle from one planet to another will in general require very long flight times. There are however some advanced trajectories involving mercury, venus, earth and mars which have remarkably short flight times and low launch energies. Since the favorable launch periods for missions to a given planet do not occure often advanced trajectories taking one free-fall vehicle to many planets are particularly attractive.

The determination of free-fall trajectories to several planets is essentially the famous unsolved n-body problem. Thus in order to calculate these trajectories certain simplifying assumptions must be made. This paper is based upon one fundamental assumption: At any instant one and only one gravitating body influences the vehicle's motion. Under this assumption almost all of the vehicle's trajectory will consist of arcs of different ellipses with the sun at a focus but when the vehicle comes sufficiently close to a passing planet its trajectory will be hyperbolic with respect to this planet while the sun's influence is neglected.

The paper contains the results of a study of such conic trajectories performed at the Jet Propulsion Laboratory during the summer of 1961. The paper also contains numerous numerical results carried out at the Computing Facility of the University of California at Los Angeles and the computing complex at the Jet Propulsion Laboratory. These calculations show that by utilizing advanced trajectories many interplanetary missions requiring very large launch vehicles could be carried out with much smaller vehicles by simply changing their mission profiles. This is particularly true for the missions to mercury and the manned missions to mars. The numerical study was confined to the decade beginning in 1965.

Contents

I. Introduction....2

II. Conic Trajectories....3

A. The $\vec{e}$ and $\vec{h}$ Vectors of Conic Trajectories....3

B. The Calculation of $\vec{e}$ and $\vec{h}$ From Two Position Vectors....7

C. Velocity Vector as a Function of $\vec{e}$, $\vec{h}$ and $\vec{R}$....9

D. Relations Between $\vec{e}$ and $\vec{h}$ and the Classical Orbital Elements....10

E. Lambert's Theorem....13

F. Extension of Kepler's Second Law of Planetary Motion....21

III. Using the Gravitational Influence of a Passing Planet....25

A. The Fundamental Equation....29

B. The Determination of the Elliptical Orbits Associated with the Transfer Trajectories....30

C. The Determination of the Hyperbolic Trajectory....34

IV. Numerical Results....40

A. Unmanned Exploration of the Inner Planets by Instrumented Space Vehicles on Advanced Trajectories....42

a. Earth-Venus-Mercury....49

b. Earth-Venus-Mars....76

B. Initial Interplanetary Missions by Manned Vehicles....91

a. Earth-Venus-Earth....91

b. Earth-Mars-Earth....92

c. Earth-Venus-Mars-Earth....94

d. Manned Landings on Venus and Mars Utilizing Advanced Trajectories....106

C. Interplanetary Transportation Networks to Support Manned Bases on Venus and Mars....118

V. Concluding Remarks....121

Appendixes

1. The Calculation of Planetary Position and Velocity Vectors....124

2. Constants of the Solar System Used in the Calculations....129

References....131

I. Introduction

It has been discovered that conic trajectories give excellent first approximations to actual flight paths of free-fall interplanetary space vehicles. Thus it is natural while studying space trajectories to assume that the vehicle moves along conic paths. The primary goal of the theoretical portion of this paper is to determine a conic trajectory in the vicinity of a passing planet which will enable the vehicle to pass out of its gravitational sphere of influence on a conic trajectory about the sun which will intercept another pre-determined planet. Thus we shall assume that the missions begin and end at the centers of massless planets. The initial conditions are given by specifying the order in which the vehicle is to rendezvous with the given planets along with the launch date and first planetary closest approach date. If these initial conditions are arbitrarily given then a solution may not exist or may be physically unrealizable; that is to say the resulting trajectory may require the vehicle to pass closer to a particular planet than its own radius.

This paper includes the results of a numerical study of these advanced trajectories performed at the Computing Facility of the University of California at Los Angeles and at the computing complex at the Jet Propulsion Laboratory. For each particular trajectory profile studied it was possible to determine those trajectories having near minimum launch energies.

The quantitative study of any branch of science dealing with forces, velocities and positions (i.e., vectors) in a 3-dimensional space is always most conveniently done by making use of as much vector analysis as possible. With this point of view no assumptions regarding the geometry of the solar system will be necessary; indeed it will not matter how eccentric the planets orbits are or how much their planes of motion differ from each other. Thus before attacking the above problem we shall first develop a convenient mathematical technique for handling conic trajectories in 3-dimensional space.

II. CONIC TRAJECTORIES

We begin our study of conic trajectories in three-dimensional space by equating the dynamic force on a space vehicle of mass m with the force of gravitional attraction set up by the presents of a body of mass M. If Σ is any inertial frame this equation becomes

$$m \frac{d\vec{V}}{dt} = -G \frac{Mm}{R^2} \hat{R}$$

where $\vec{V}$ is the velocity of the vehicle and $\hat{R}$ is a unit vector directed from the center of the body to the vehicle separated by a distance R. We shall adhere to the convention of denoting unit vectors by placing Λ over the letter.

Since the ratio m/M is very small we may assume that the body is at rest in Σ. We shall take the center of this body as the origin of Σ. By setting $GM = \mu$ and cancelling out m from both sides of the above equation we obtain

$$\frac{d\vec{V}}{dt} = -\frac{\mu}{R^2} \hat{R} \qquad (1)$$

A. The $\vec{e}$ and $\vec{h}$ Vectors of Conic Trajectories

By the differentation formula for the cross product of two vectors we write

$$\frac{d}{dt} (\vec{R} \times \vec{V}) = \frac{d\vec{R}}{dt} \times \vec{V} + \vec{R} \times \frac{d\vec{V}}{dt} .$$

Hence with the aid of (1) we have

$$\frac{d}{dt} (\vec{R} \times \vec{V}) = 0$$

since the cross product of paralled vectors vanish. This result implies

$$\vec{R} \times \vec{V} = \int \frac{d}{dt} (\vec{R} \times \vec{V}) \, dt + \vec{h} = \vec{h}$$

where $\vec{h}$ is a constant vector of integration.

$$\vec{R} \times \vec{V} = \vec{h} \tag{2}$$

From this important relation we notice that $\vec{R}$ always remains perpendicular to $\vec{h}$ and consequently the motion remains confined to a fixed plane in Σ. The angular momentum of the vehicle about the body is simply $m\vec{h}$.

We now express (2) in a slightly different form :

$$\vec{h} = \vec{R} \times \frac{d\vec{R}}{dt} = \vec{R} \times \frac{d}{dt} (R \overset{\Lambda}{R}) = R \times \left(\frac{dR}{dt} \overset{\Lambda}{R} + R \frac{d\overset{\Lambda}{R}}{dt} \right)$$

Thus

$$\vec{h} = R^2 \overset{\Lambda}{R} \times \frac{d\overset{\Lambda}{R}}{dt}$$

employing this result with (1) we find

$$\frac{d\vec{V}}{dt} \times \vec{h} = -\mu \overset{\Lambda}{R} \times \left(\overset{\Lambda}{R} \times \frac{d\overset{\Lambda}{R}}{dt} \right)$$

and after applying the vector triple product formula of vector analysis we have

$$\frac{d\vec{V}}{dt} \times \vec{h} = -\mu \left[\left(\overset{\Lambda}{R} \cdot \frac{d\overset{\Lambda}{R}}{dt} \right) \overset{\Lambda}{R} - \left(\overset{\Lambda}{R} \cdot \overset{\Lambda}{R} \right) \frac{d\overset{\Lambda}{R}}{dt} \right] .$$

Now since $\overset{\Lambda}{R} \cdot \overset{\Lambda}{R} = 1$

$$\overset{\Lambda}{R} \cdot \frac{d\overset{\Lambda}{R}}{dt} = \frac{1}{2}\left(\overset{\Lambda}{R} \cdot \frac{d\overset{\Lambda}{R}}{dt} + \frac{d\overset{\Lambda}{R}}{dt} \cdot \overset{\Lambda}{R}\right) = \frac{1}{2}\frac{d}{dt}\left(\overset{\Lambda}{R} \cdot \overset{\Lambda}{R}\right) = 0 .$$

Consequently

$$\frac{d\vec{V}}{dt} \times \vec{h} = \mu \frac{d\overset{\Lambda}{R}}{dt} .$$

By noting that $\vec{h}$ is a constant vector and μ is a constant scalor this equation may be written as

$$\frac{d}{dt}\left(\vec{V} \times \vec{h}\right) = \frac{d}{dt}\left(\mu \overset{\Lambda}{R}\right)$$

whereupon an integration leads to

$$\vec{V} \times \vec{h} = \mu \overset{\Lambda}{R} + \vec{c}$$

where $\vec{c}$ is another constant vector of integration. By setting

$$\vec{c} = \mu \vec{e}$$

we obtain

$$\vec{V} \times \vec{h} = \mu \left(\overset{\Lambda}{R} + \vec{e}\right) \qquad (3)$$

where $\vec{e}$ is some constant vector. This vector can be expressed as

$$\vec{e} = \frac{1}{\mu} \vec{V} \times \vec{h} - \hat{R} \tag{4}$$

which follows directly from (3). Since $\vec{V} \times \vec{h}$ is a vector lying in the plane of motion the above relation implies that $\vec{e}$ lies in the plane of motion also.

Let θ be the angle measured from $\vec{e}$ in the positive direction (i.e., counterclockwise) to $\vec{R}$. Hence in view of (2) and (3) we have

$$h^2 = \vec{h} \cdot \vec{h} = \vec{h} \cdot \vec{R} \times \vec{V} = \vec{R} \cdot \vec{V} \times \vec{h} = \vec{R} \cdot \mu \, (\hat{R} + \vec{e}) \, .$$

Thus

$$\frac{h^2}{\mu} = R + R \, e \cos \theta = R \, (1 + e \cos \theta) \, .$$

Consequently we obtain

$$R = \frac{\frac{h^2}{\mu}}{1 + e \cos \theta} \, . \tag{5}$$

This is the general equation of a conic with eccentricity e and semi-latus rectum

$$\ell = \frac{h^2}{\mu} \tag{6}$$

$$R = \frac{\ell}{1 + e \cos \theta} \tag{7}$$

Thus we obtain the well-known fact that the trajectory is a conic section.

Since (7) implies that R is smallest when $\theta = 0$, the direction of $\vec{e}$ is along the direction of perihelion (see figure 1).

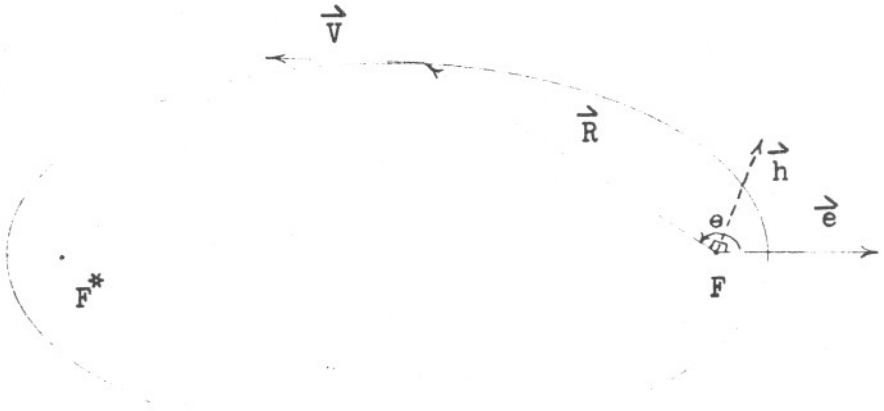

Figure 1

B. <u>The Calculation of $\vec{e}$ and $\vec{h}$ Vectors From Two Postion Vectors</u>

If two position vectors on an elliptic trajectory are known along with its semi-major axis a and eccentricity e the $\vec{e}$ and $\vec{h}$ vectors can be calculated. The $\vec{h}$ vector can easily be obtained from

$$\vec{h} = \pm \frac{\vec{R}_1 \times \vec{R}_2}{\left| \vec{R}_1 \times \vec{R}_2 \right|} \sqrt{a \mu \left| 1-e^2 \right|} \qquad (8)$$

where the choice of signs depends upon $\measuredangle$ $\vec{R}_1$, $\vec{R}_2$ and the direction of motion. The calculation of the $\vec{e}$ vector can be carried out by the following formula:

$$\vec{e} = \alpha \vec{R}_1 + \beta \vec{R}_2 \qquad (9)$$

where

$$\alpha = \frac{\begin{vmatrix} b_1 & a_{12} \\ b_2 & a_{22} \end{vmatrix}}{D} \qquad \beta = \frac{\begin{vmatrix} a_{11} & b_1 \\ a_{21} & b_2 \end{vmatrix}}{D} \tag{10}$$

with

$$\left.\begin{aligned} b_i &= \frac{\ell}{R_i} + e^2 - 1 \\ a_{ii} &= \ell \\ a_{ij} &= \hat{R}_i \cdot \vec{R}_j + \ell - R_j \qquad i \neq j \end{aligned}\right\} \tag{11}$$

and

$$D = \begin{vmatrix} a_{11} & a_{12} \\ a_{21} & a_{22} \end{vmatrix} \tag{12}$$

The derivation of (8) is omitted since it is immediately obvious but (9) along with (10), (11) and (12) is more involved. These formulas can be established by first noting that since the e vector lies in the plane of motion, two scalors α and β exist such that (9) holds. If we denote the vehicles velocity vectors at $\vec{R}_1$ and $\vec{R}_2$ by $\vec{V}_1$ and $\vec{V}_2$ respectively and dot each side of (9) by $\frac{1}{\mu}\ \vec{V}_1 \times \vec{h}$ and $\frac{1}{\mu}\ \vec{V}_2 \times \vec{h}$ we obtain the following equations

$$\frac{1}{\mu}\ \vec{V}_1 \times \vec{h}\cdot\vec{e} = \frac{1}{\mu}\ \vec{V}_1 \times \vec{h}\cdot\vec{R}_1\alpha + \frac{1}{\mu}\vec{V}_1 \times \vec{h}\cdot\vec{R}_2\ \beta$$

$$\frac{1}{\mu}\ \vec{V}_2 \times \vec{h}\cdot\vec{e} = \frac{1}{\mu}\ \vec{V}_2 \times \vec{h}\cdot\vec{R}_1\alpha + \frac{1}{\mu}\vec{V}_2 \times \vec{h}\cdot\vec{R}_2\ \beta\ .$$

By employing (3) and noting that (7) implies

$$\overset{\Lambda}{R}\cdot\vec{e} = \frac{\ell}{R} - 1$$

the formulas (10), (11) and (12) can easily be seen to follow.

C. Velocity Vector as a Function of $\vec{e}$, $\vec{h}$ and $\vec{R}$

We now come to a very useful formula which expresses the vehicles velocity vector in terms of the e and h vectors and its unit position vector $\overset{\Lambda}{R}$. The derivation follows by making use of the vector tripal product formula

$$\vec{h} \times (\vec{V} \times \vec{h}) = (\vec{h}\cdot\vec{h})\ \vec{V} - (\vec{h}\cdot\vec{V})\ \vec{h}\ .$$

Thus since $\vec{V}$ is perpendicular to $\vec{h}$ we have

$$h^2\ \vec{V} = \vec{h} \times (\vec{V} \times \vec{h})$$

and hence by employing (3) we obtain

$$\vec{V} = \frac{\mu}{h^2}\ \vec{h} \times (\overset{\Lambda}{R} + \vec{e})\ . \qquad (13)$$

As an immediate application of (13) we now derive the well-known energy equation. With the aid (13) together with (6) we may write

$$V^2 = \frac{1}{\ell} \quad (\vec{V} \cdot \vec{h} \times \hat{R} + \vec{V} \cdot \vec{h} \times \vec{e}) .$$

By the box product formulas this becomes

$$V^2 = \frac{1}{R\ell} \quad \left[\vec{h} \cdot \vec{R} \times \vec{V} + R\,(\vec{e} \cdot \vec{V} \times \vec{h})\right] .$$

After making use of (2) and (3) this can be written as

$$V^2 = \frac{1}{R\ell} \quad \left[h^2 + \mu\,(R\,e\cos\theta + R\,e^2)\right] .$$

Consequently with the aid of (5) this is expressable as

$$V^2 = \frac{1}{R\ell} \quad \left[2h^2 + \mu R\ (e^2 - 1)\right]$$

and by (6) we obtain the famous energy equation

$$V^2 = \mu\left(\frac{2}{R} \mp \frac{1}{a}\right) \tag{14}$$

where the negative or positive sign is chosen according to whether the trajectory is elliptic or hyperbolic.

D. Relations between the e and h Vectors and Classical Orbital Elements

The vectors $\vec{e}$ and $\vec{h}$ along with the time of perhelion passage T_p completely determines the conic trajectory. These vectors represent six constant scalors five of which are independent. To an astronomer, who is primarily interested in knowing where to point his telescope, the old method of defining an orbit by giving its classical orbital elements Ω, i, ω, a, e, T_p is very convenient. But in Astronautics velocity vectors

play an important roll. The determination of velocity vectors of celestial bodies, having orbits defined by the classical osculating elements usually requires slow and cumbersome numerical differentation of position vectors. By defining the trajectories in terms of osculating e and h vectors, velocity vectors can be immediately calculated by (13).

The classical orbital elements can easily be calculated for a trajectory described by $\vec{e}$, $\vec{h}$ and T_p by referring to figure 2 where Σ is taken to be an ecliptic coordinate system.

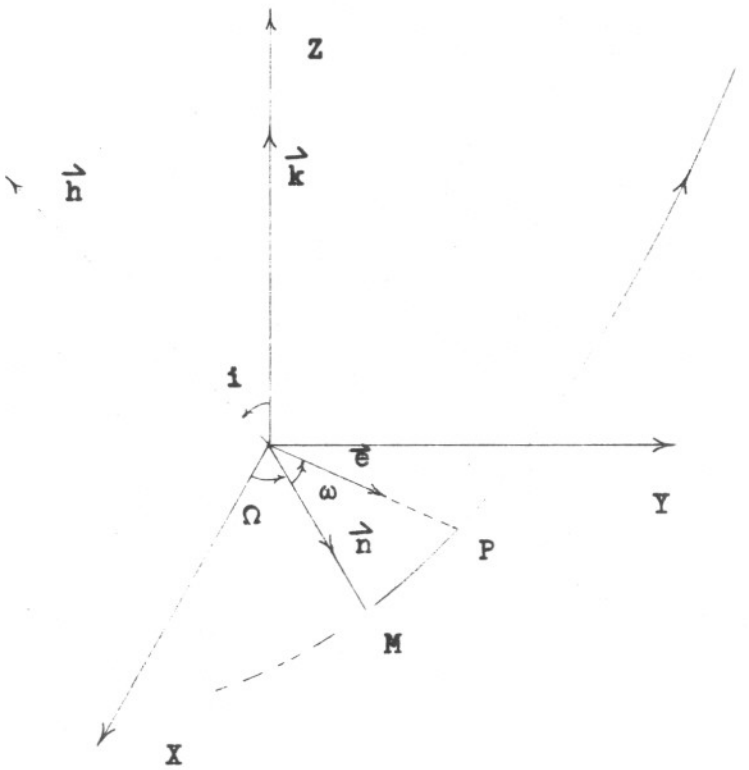

Figure 2

We take M to denote the point where the vehicle rises above the ecliptic which is the x y plane and $\hat{n}$ as a unit vector directed toward M. The point of perihelion is denoted by P. The x axis is directed toward the vernal equinox for some epoch.

Now the time of perihelion passage T_P is already given and $|\vec{e}| = e$. Thus, only four of the six orbital elements remain to be calculated. From (6) the semi-major axis a can be obtained by

$$a = \frac{h^2}{\mu \left|1-e^2\right|} \quad .$$

The inclination i of the trajectory can be calculated from the relation

$$\cos i = \frac{h_3}{h} \tag{15}$$

where we write $\vec{h} = (h_1, h_2, h_3)$ and $\vec{e} = (e_1, e_2, e_3)$. The unit vector $\hat{n}$ is given by

$$\hat{n} = (\cos \Omega, \sin \Omega, 0)$$

consequently since

$$\hat{k} \times \vec{h} = h \sin i \; \hat{n}$$

The longitude of the ascending node can be obtained by

$$\sin \Omega = \frac{h_1}{h \sin i} \qquad \cos \Omega = \frac{-h_2}{h \sin i} \tag{16}$$

The argument of perihelion ω may be calculated from

$$\cos \omega = \frac{\hat{n} \cdot \vec{e}}{e} \tag{17}$$

Similarly one easily finds that if a trajectory is defined by the classical orbital elements, the e and h vectors can be calculated by the following formulas:

$$e_1 = e(\cos \Omega \cos \omega - \cos i \sin \Omega \sin \omega) \tag{18}$$

$$e_2 = e(\sin \Omega \cos \omega + \cos i \cos \Omega \sin \omega) \tag{19}$$

$$e_3 = e \sin i \sin \omega \tag{20}$$

$$h_1 = h \sin i \sin \Omega \tag{21}$$

$$h_2 = -h \sin i \cos \Omega \tag{22}$$

$$h_3 = h \cos i \tag{23}$$

where $h = \sqrt{\mu a \left|1-e^2\right|}$

E. Lambert's Theorem

We now come to a fundamental theorem of Celestial mechanics known as Lambert's Theorem. This profound result will play an important roll in the determination of interplanetary trajectories. The theorem states that the time required for a body to move from a point P with position vector $\vec{R}_1$ to a point Q with position vector $\vec{R}_2$ depends only on $R_1 + R_2$ and the distance c between P and Q.

The proof of this theorem can be readily found in any advanced text on Celestial Mechanics (see for example reference 2) and hence we shall merely state the associated equations which correspond to elliptical trajectories.

Let a body moving on an elliptic path be at the points P at time T_1 and Q at T_2. If the arc $\overline{PQ}$ traversed by the body during the time interval $T = T_2 - T_1$ is less than 180°, then if F and F^* denotes the occupied and vacant foci respectively

$$T = \sqrt{\frac{a^3}{\mu}} \left\{ \sqrt{1 - x_2^2} + \sin^{-1} x_2 - \sqrt{1 - x_1^2} - \sin^{-1} x_1 \right\} \qquad (24)$$

provided the line segment $\overline{PQ}$ does not intersect $\overline{FF^*}$ and

$$T = \sqrt{\frac{a^3}{\mu}} \left\{ \pi + \sqrt{1 - x_2^2} + \sin^{-1} x_2 + \sqrt{1 - x_1^2} + \sin x_1 \right\} \qquad (25)$$

if $\overline{PQ}$ does intersect $\overline{FF^*}$ shere

$$x_1 = 1 - \frac{s}{a}, \quad x_2 = 1 - \frac{s-c}{a} \quad \text{and} \quad s = \frac{1}{2} (\overline{FP} + \overline{FQ} + c).$$

The geometry of these two situations is shown in figure 3. By taking P and Q to be perihelion and aphelion we find that the period P of the trajectory is

$$P = 2\pi \sqrt{\frac{a^3}{\mu}}$$

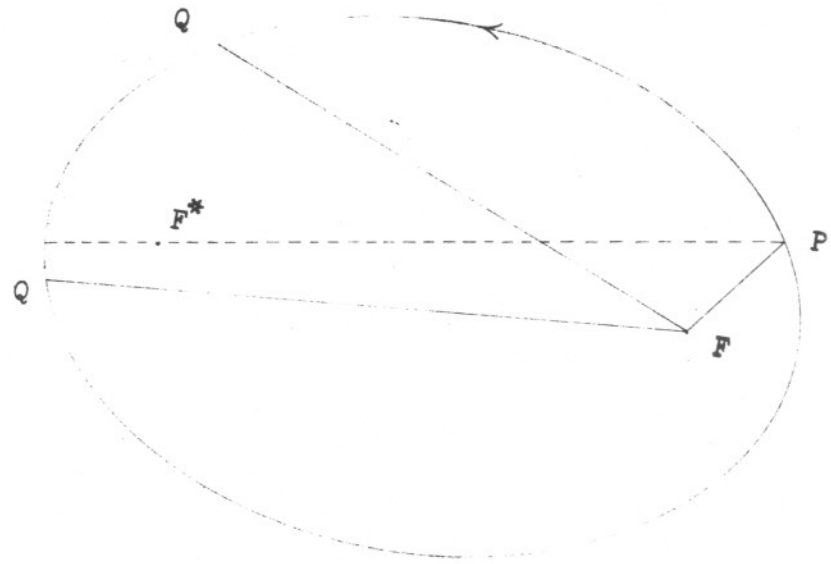

Figure 3

Consequently if arc $\overline{PQ}$ subtended by P and Q lies in the range $\left[180^\circ, 360^\circ\right]$, (24) becomes

$$T = \sqrt{\frac{a^3}{\mu}} \left\{ 2\pi - \sqrt{1 - x_2^2} - \sin x_2 + \sqrt{1 - x_1^2} + \sin x_1 \right\} \qquad (26)$$

and (25) becomes

$$T = \sqrt{\frac{a^3}{\mu}} \left\{ \pi - \sqrt{1 - x_2^2} - \sin x_2 - \sqrt{1 - x_1^2} - \sin^{-1} x_1 \right\} \qquad (27)$$

If on the other hand we assume that the angle subtended by P and Q lies in the range $\left[360^\circ, 540^\circ\right]$, (24) and (25) become

$$T = \sqrt{\frac{a^3}{\mu}} \left\{ 2\pi + \sqrt{1 - x_2^2} + \sin^{-1} x_2 - \sqrt{1 - x_1^2} - \sin^{-1} x_1 \right\} \qquad (28)$$

$$T = \sqrt{\frac{a^3}{\mu}} \left\{ 3\pi + \sqrt{1 - x_2^2} + \sin^{-1} x_2 + \sqrt{1 - x_1^2} + \sin^{-1} x_1 \right\} \qquad (29)$$

respectively. The eccentricity of the elliptic path corresponding to the case where $\overline{PQ}$ does not intersect $\overline{Fr^*}$ is given by

$$e = \left\{ 1 - \frac{2}{c^2} (s - \overline{FP}) (S - \overline{FQ}) (1 - x_1 x_2 + \sqrt{1 - x_1^2}\sqrt{1 - x_2^2}) \right\}^{\frac{1}{2}} \qquad (30)$$

If $\overline{PQ}$ does intersect $\overline{Fr^*}$

$$e = \left\{ 1 - \frac{2}{c^2} (S - \overline{FP}) (S - \overline{FQ}) (1 - x_1 x_2 - \sqrt{1 - x_1^2}\sqrt{1 - x_2^2}) \right\}^{\frac{1}{2}} \qquad (31)$$

Interplanetary conic trajectories of free-fall space vehicles in the foreseeable future will be elliptical. Thus if such a vehicle is to move along an elliptical path leaving P at time T_1 and arriving at Q at the time T_2, the semi-major axis a of the trajectory may be calculated by one of the formulas (24) - (29) provided of course the angle subtended by P and Q is not greater than 540°.

The eccentricity can then be calculated by (30) or (31). Thus recalling part B of section II the corresponding e and h vectors can be calculated and hence the trajectory can be completely determined.

Now let us suppose that the point P represents a launch planet moving with velocity $\vec{V}_p$ at T_1 when the vehicle is launched. If at this moment the vehicle's velocity vector is $\vec{V}$ with respect to the sun and $\vec{V}'$ with respect to P we have

$$\vec{V} = \vec{V}_p + \vec{V}'$$

Consequently

$$V'^2 = \vec{V}' \cdot \vec{V}' = (\vec{V} - \vec{V}_p) \cdot (\vec{V} - \vec{V}_p) = V^2 - 2\vec{V} \cdot \vec{V}_p + V_p^2$$

or if $\measuredangle \vec{V}, \vec{V}_p = \theta$

$$V'^2 = V^2 - 2V V_p \cos\theta + V_p^2 \qquad (32)$$

Thus by the energy equation (32) may be expressed as

$$V'^2 = \sqrt{\mu\left(\frac{2}{\overline{FP}} - \frac{1}{a}\right)}\left(\sqrt{\mu\left(\frac{2}{\overline{FP}} - \frac{1}{a}\right)} - 2V_p \cos\theta\right) + V_p^2$$

which implies that V' is minimum when $\theta = 0$ and a is minimum. From the definition of an ellipse we may write

$$\overline{FP} + \overline{F^*P} = 2a$$

$$\overline{FQ} + \overline{F^*Q} = 2a$$

Hence we may write

$$2S = \overline{FP} + \overline{FQ} + c = (\overline{FP} + \overline{F^*P}) + (\overline{FQ} + \overline{F^*Q}) + (c - \overline{F^*P} - \overline{F^*Q}).$$

Thus

$$2S + \overline{F^*P} + \overline{F^*Q} - c = 4a$$

and since the sum of any two sides of a plane triangle is greater than or equal to the third side we find

$$a > \frac{s}{2}$$

The above results show that minimum launch energy trajectories have $\theta = 0$ and $a = \frac{s}{2}$ where s is minimum (i.e. $s = \overline{FP} + \overline{FQ}$ or equivalently when $c = \overline{FP} + \overline{FQ}$). These minimum launch energy trajectories are also referred to as Hohmann transfers. Figure 4 describes Hohmann transfers to venus and mars. Consequently it is important to have a general idea of the properties of the functions (24)-(29). It is particularly important to know how these functions compare with each other.

Consider the set of all pairs of points P, Q such that $\overline{FP} + \overline{FQ}$ and c remain unchanged along with the occupied focus F. Through each pair of points let us pass all possible elliptical paths such that $0 \leq \measuredangle PFQ \leq 540^\circ$ by varying the semi-major axis and the eccentricity. The graphs of T vs. a of the six functions can then be plotted for identical values of $\overline{FP} + \overline{FQ}$ and c.

Figure 6 is an example of how these functions behave.

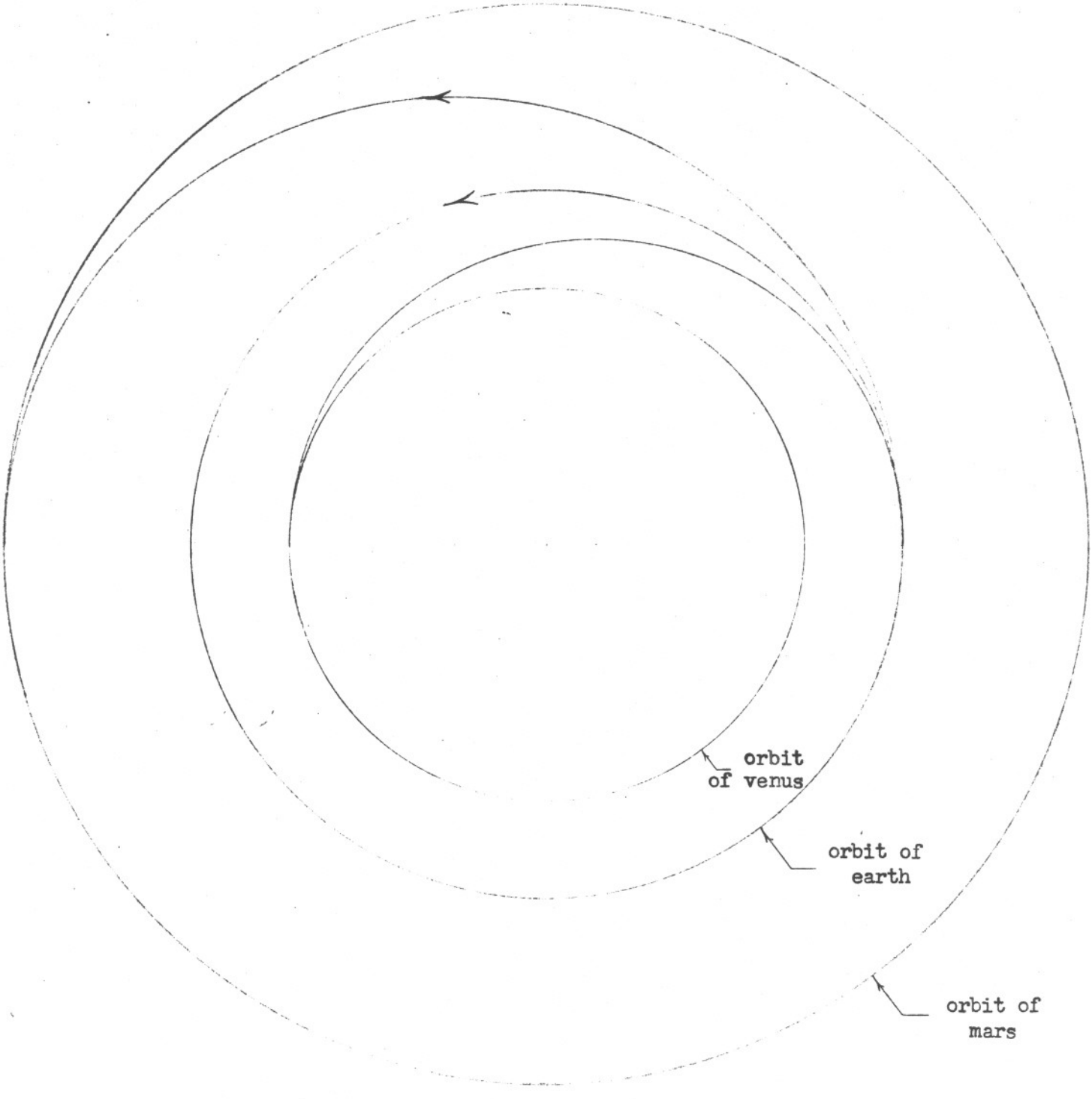

Figure 4

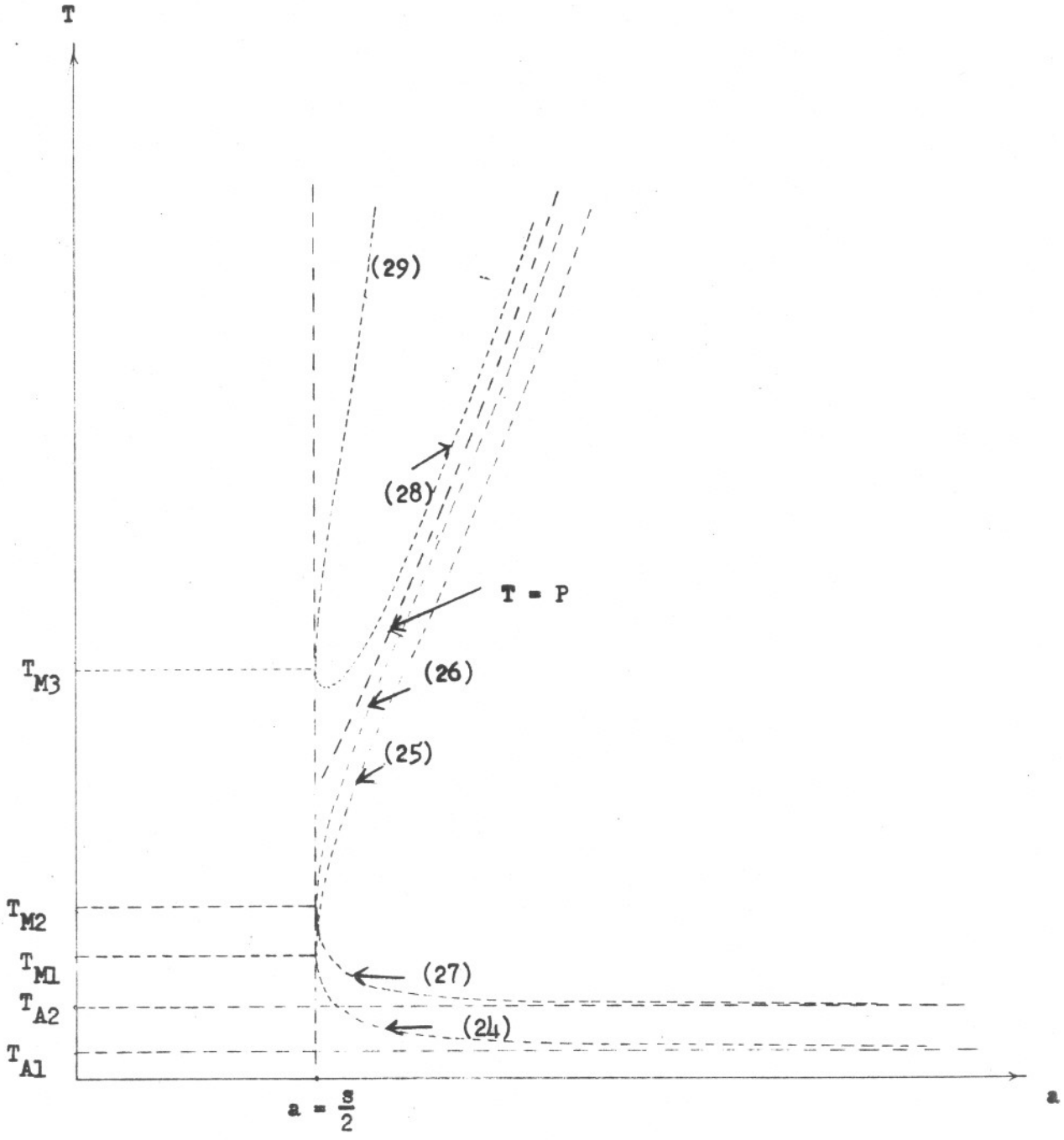

Figure 6

In the above figure T_{A1} and T_{A2} are asymptotic values which can be shown to be

$$T_{A1} = \frac{1}{3}\sqrt{\frac{2}{\mu}}\left\{\sqrt{s^3} - \sqrt{(s-c)^3}\right\}$$

$$T_{A2} = \frac{1}{3}\sqrt{\frac{2}{\mu}}\left\{\sqrt{s^3} + \sqrt{(s-c)^3}\right\}$$

When a = mimimum = $\frac{s}{2}$, the graph of (24) joins (25) at time T_{M1} and the graph of (26) joins (27) at time T_{M2} and the graph of (28) joins (29) at time T_{M3}. By substituting $a = \frac{s}{2}$ into (24) or (25) we find

$$T_{M1} = \sqrt{\frac{s^3}{2\mu}}\left\{\sqrt{\frac{c}{s}\left(1 - \frac{c}{s}\right)} + \frac{1}{2}\sin^{-1}\left(\frac{2c}{s} - 1\right) + \frac{\pi}{4}\right\}$$

and substituting $a = \frac{s}{2}$ into (26) or (27) yields

$$T_{M2} = \sqrt{\frac{s^3}{2\mu}}\left\{\frac{3\pi}{4} - \sqrt{\frac{c}{s}\left(1 - \frac{c}{s}\right)} - \frac{1}{2}\sin^{-1}\left(\frac{2c}{s} - 1\right)\right\}$$

Since $T_{M3} = T_{M1} + P\left(a = \frac{s}{2}\right)$ we have

$$T_{M3} = \sqrt{\frac{s^3}{2\mu}}\left\{\sqrt{\frac{c}{s}\left(1 - \frac{c}{s}\right)} + \frac{1}{2}\sin^{-1}\left(\frac{2c}{s} - 1\right) + \frac{5}{4}\pi\right\}$$

F. Extension of Kepler's Second Law of Planetary Motion

The second of Kepler's three laws of Planetary motion states that the radius vector from the sun to a planet sweeps out equal areas in equal times. We shall now show that this law also applies to parabolic and hyperbolic paths.

Let π denote the plane of motion of a body moving under the influence of one and only one other body. Let $\vec{h}$ denote the resulting h-vector of the conic trajectory.

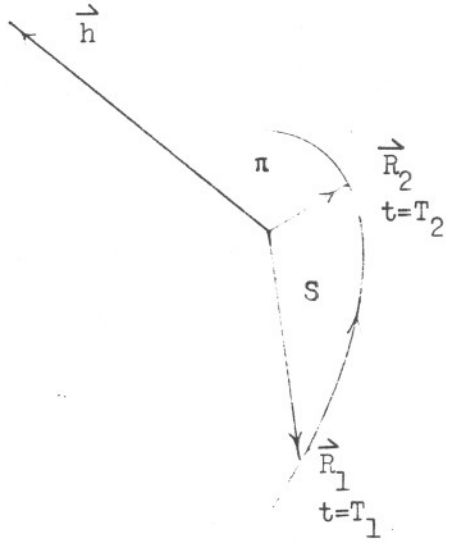

Figure 7

Let S denote the area of π bounded by the arc of the trajectory and the radius vectors $\vec{R}\,(T_1)$ and $\vec{R}(T_2)$. If C denotes the boundary of S we write by Stokes' theorem

$$\oint_C \vec{f} \cdot d\vec{R} = \iint_S \hat{h} \cdot (\nabla \times \vec{f})\, dS$$

where $\vec{f}$ is any vector function having continuous gradient Δf over S. letting

$$\vec{f} = \vec{\zeta} \times \vec{R}$$

where $\vec{\zeta}$ is any arbitrary constant vector we may write

$$\oint_C (\vec{\zeta} \times \vec{R}) \cdot d\vec{R} = \iint_S \hat{h} \cdot \nabla \times (\vec{\zeta} \times \vec{R})\, dS. \qquad (33)$$

With the aid of the box product formulas it follows that

$$\vec{\zeta} \times \vec{R} \cdot d\vec{R} = d\vec{R} \cdot \vec{\zeta} \times \vec{R} = \vec{\zeta} \cdot \vec{R} \times d\vec{R}$$

Recalling the formula for the curl of a cross product of two vector functions we write

$$\nabla \times (\vec{\zeta} \times \vec{R}) = \vec{R} \cdot \nabla \vec{\zeta} - \vec{\zeta} \cdot \nabla \vec{R} + \vec{\zeta} \nabla \cdot \vec{R} - \vec{R} \nabla \cdot \vec{\zeta}.$$

Since $\vec{\zeta}$ is a const vector the dyadic $\nabla\vec{\zeta}$ and the scalor $\nabla \cdot \vec{\zeta}$ vanish. Also since $\vec{R} = x\,\hat{i} + y\,\hat{i} + Z\,\hat{k}$, the dyadic $\nabla \vec{R}$ is the idemfactor I for

$$\nabla \vec{R} = \frac{\partial \vec{R}}{\partial x}\hat{i} + \frac{\partial \vec{R}}{\partial y}\hat{i} + \frac{\partial \vec{R}}{\partial z}\hat{k} = \hat{i}\,\hat{i} + \hat{j}\,\hat{j} + \hat{k}\,\hat{k} = I.$$

Thus by noting that $\Delta \cdot \vec{R} = 3$ we obtain

$$\nabla \times (\vec{\zeta} \times \vec{R}) = -\vec{\zeta} \cdot I + 3\vec{\zeta} = 2\vec{\zeta}.$$

By substituting these results into (33) one finds

$$\vec{\zeta} \cdot \oint_C \vec{R} \times d\vec{R} = 2\vec{\zeta} \cdot \hat{h} \iint_S ds = 2\vec{\zeta} \cdot \hat{h}\, S.$$

Now $\vec{\zeta}$ is any arbitrary constant vector, hence it follows from the above equation that

$$\oint_C \vec{R} \times d\vec{R} = 2\hat{h}\, S.$$

Since

$$d\vec{R} = \frac{d\vec{R}}{dt}\, dt = \vec{V} dt$$

the equation can be written as

$$\int_{T_1}^{T_2} \vec{R} \times \vec{V}\, dt = 2\, \overset{\Lambda}{h}\, S.$$

By employing (2) this result reduces to

$$h\,(T_2 - T_1) = 2\,S.$$

Hence Kepler's second law of planetary motion holds for all conic trajectories.

Let $T = T_2 - T_1$ where T_1 is the time of perihelion passage. Then by the above result we may write

$$T = \frac{2S}{h} = \frac{1}{h} \int_0^{\theta} R^2\, d\,\theta. \tag{34}$$

Since (5) and (6) imply

$$d\,\theta = \frac{\ell}{R^2\, e \sin \theta}\, dR$$

we obtain

$$T = \frac{\ell}{eh} \int_{R_o}^{R} \frac{dR}{\sqrt{1 - \left(\frac{\ell}{R} - 1\right)^2 \frac{1}{e^2}}} \tag{35}$$

where $R_o = a\,(1 - e)$ for elliptical trajectories and $R_o = a\,(e - 1)$ for hyperbolic trajectories. The integral can be integrated in closed form.

III. Using the Gravitational Influence of a Passing Planet.

The effort taking place in the development of space vehicles designed for the exploration of the solar system is rapidly gaining momentum. Recent advances in many fields such as metallurgy, chemistry and electronics are being applied to actual hardware as soon as they become available. With the arrival of new sophisticated long life interplanetary spacecraft many new complex deep space operations will be possible. Such vehicles equiped with an advanced planetary approach guidance system could accurately control its entry into the vicinity of a passing planet. If the mission does not require the vehicle to land or to orbit the planet the small guidance package along with the planets gravitational influence gives the vehicle the potential of radically changing its trajectory about the sun.

We now consider the problem of finding a conic approximation of the trajectory of a free fall vehicle in the vicinity of a passing planet such that its influence will enable the vehicle to rendezvous with another planet. Let Σ denote any cartesion inertial frame with the sun's center as its origin. Let Σ' be a parallel translation of Σ with new origin located at the center of a planet influencing the motion of the vehicle. Let τ denote the region of gravitational influence about the planet. It can be shown that τ can be taken as a spherical region with center at the planets center and radius ρ^* given by

$$\rho^* = \left(\frac{m}{M}\right)^{\frac{2}{5}} R$$

where R is the distance between the sun of mass M and the planet of mass m.

The problem is formally stated as follows:

Suppose a free fall interplanetary space vehicle leaves a planet P_1 at time T_1 and makes a closest approach to a planet P_2 at time T_2. The influence of P_2 then causes the

vehicle to rendezvous with a third planet P_3 (P_3 may or may not be P_1 indeed it may be another space vehicle orbiting the sun). The planets P_1, P_2 and P_3 along with T_1 and T_2 are given. The elliptical transfer trajectory from P_1 to P_2, the hyperbolic trajectory in τ, and the elliptical transfer trajectory from P_2 to P_3 at time T_3 are to be determined.

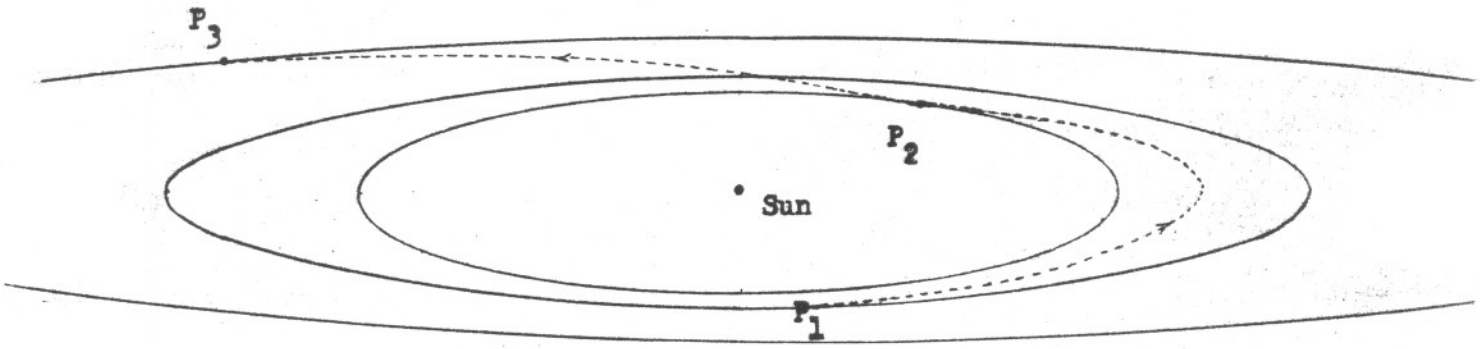

Figure 8

The following notation shall be employed throughout this section:

(a) $\overset{\frown}{P_1 P_2}$ = the elliptical transfer trajectory from P_1 to P_2

(b) $\overset{\frown}{P_2 P_3}$ = the elliptical transfer trajectory from P_2 to P_3

(c) $\vec{R}_i(t)$ = position vector of P_i with respect to Σ at time t ($i = 1,2,3$)

(d) $\vec{R}(t)$ = position vector of vehicle with respect to Σ at time t

(e) $\vec{\rho}(t)$ = position vector of vehicle with respect to Σ' at time t

(f) $\vec{V}_i(t)$ = velocity vector of P_i with respect to Σ at time T ($i = 1,2,3$)

~~(g) $\vec{V}_i$ = velocity vector of P_i with respect to Σ at time T_i~~

(h) $\vec{V}(t)$ = velocity vector of vehicle with respect to Σ at time t

(i) $\vec{V}'(t)$ = velocity vector of vehicle with respect to Σ' at time t

(j) T_1^*, T_2^* = time at which vehicle enters and leaves τ respectively

(k) a_1, ℓ_1; a_3, ℓ_3 = semi-major axis and semi-latus rectum of $\overset{\frown}{P_1 P_2}$ and $\overset{\frown}{P_2 P_3}$ respectively

(l) $\vec{e}_1$, $\vec{h}_1$; $\vec{e}_3$, $\vec{h}_3$ = E and H vectors of $\overset{\frown}{P_1 P_2}$ and $\overset{\frown}{P_2 P_3}$ respectively

(m) a_2, $\vec{e}_2$, $\vec{h}_2$ = semi-major axis and E and H vectors of hyperbolic trajectory in τ with respect to Σ' (with respect to Σ, the trajectory in τ is not a conic and hence these quantities have no meaning)

~~(n) R_2 = radius of P_2~~

(o) d = distance of closest approach to the surface of P_2

(p) $\mu_2 = m_2 G$ where m_2 is the mass of P_2 and G is the gravitational constant

For definiteness we shall assume that $\measuredangle \vec{R}_1(T_1), \vec{R}_2(T_2)$ and $\measuredangle R_2(T_2), R_3(T_3)$ are not greater than 540° so that one of the formulas (24) - (29) will always be applicable.

A. The Fundamental Equation

If $T_1^* < t < T_2^*$ it follows from the above notations that

$$\vec{R}(t) = \vec{R}_2(t) + \vec{\rho}(t)$$

whence by differentiation

$$\vec{V}(t) = \vec{V}_2(t) + \vec{V}'(t)$$

Since half of the total time that the vehicle spends in τ is very small compared to the period of P_2 about the sun we may write

$$\vec{V}(t) = \vec{V}_2 + \vec{V}'(t)$$

and consequently

$$\vec{V}(T_i^*) = \vec{V}_2 + \vec{V}'(T_i^*) \qquad (i = 1,2) \qquad (36)$$

Since $V^2 = \vec{V} \cdot \vec{V}$ these equations yield

$$V^2(T_i^*) = V^2{}_2 + 2\vec{V}_2 \cdot \vec{V}'(T_i^*) + V'^2(T_i^*) \qquad (37)$$

By invoking the energy equation (14) for hyperbolic trajectories we write

$$V'^2(T_i^*) = \mu_2 \left(\frac{2}{\rho(T_i^*)} + \frac{1}{a_2} \right)$$

The radius of τ at T_1^* which is $\rho\,(T_1^*)$ is almost identical with the radius of τ at T_2^* which is $\rho\,(T_2^*)$. Thus the above equation implies that the vehicles energy with respect to Σ' as it enters τ is the same as its energy as it leaves τ.

$$V'^2\,(T_1^*) = V'^2\,(T_2^*) \tag{38}$$

Upon substituting this result into the difference of the equations given by (37) we find

$$V^2\,(T_2^*) - V^2\,(T_1^*) = 2\,\vec{V}_2 \cdot \left(\vec{V}'\,(T_2^*) - \vec{V}'\,(T_1^*)\right) \tag{39}$$

Taking the difference of the two equations given by (36) we have

$$\vec{V}'\,(T_2^*) - \vec{V}'\,(T_1^*) = \vec{V}\,(T_2^*) - \vec{V}\,(T_1^*)$$

and substituting this result into (39) we obtain an important equation by which all three parts of the total trajectory can be determined.

$$V^2\,(T_2^*) - V^2\,(T_1^*) = 2\,\vec{V}_2 \cdot \left(\vec{V}\,(T_2^*) - \vec{V}\,(T_1^*)\right) \tag{40}$$

It should be born in mind that this equation in essence says nothing more than (38) Its value lies in its form where the quantities are given with respect to Σ and not Σ'.

B. The Determination of the Elliptical Orbits Associated with the Transfer Trajectories.

By the orbits associated with the transfer trajectories we mean the two closed elliptical orbits about the sun where $\overset{\frown}{P_1 P_2}$ and $\overset{\frown}{P_2 P_3}$ are sections. The elliptical trajectory $\overset{\frown}{P_1 P_2}$ begins at the center of P_1 with position vector $\vec{R}_1\,(T_1)$ and ends at a point on the surface of τ at T_1^* with position vector $\vec{R}\,(T_1^*)$. The elliptical trajectory

$\overset{\frown}{P_2 P_3}$ begins at a point on the surface of τ at T_2^* with position vector $\vec{R}\,(T_2^*)$ and ends at the center of P_3 with position vector $\vec{R}_3\,(T_3)$.

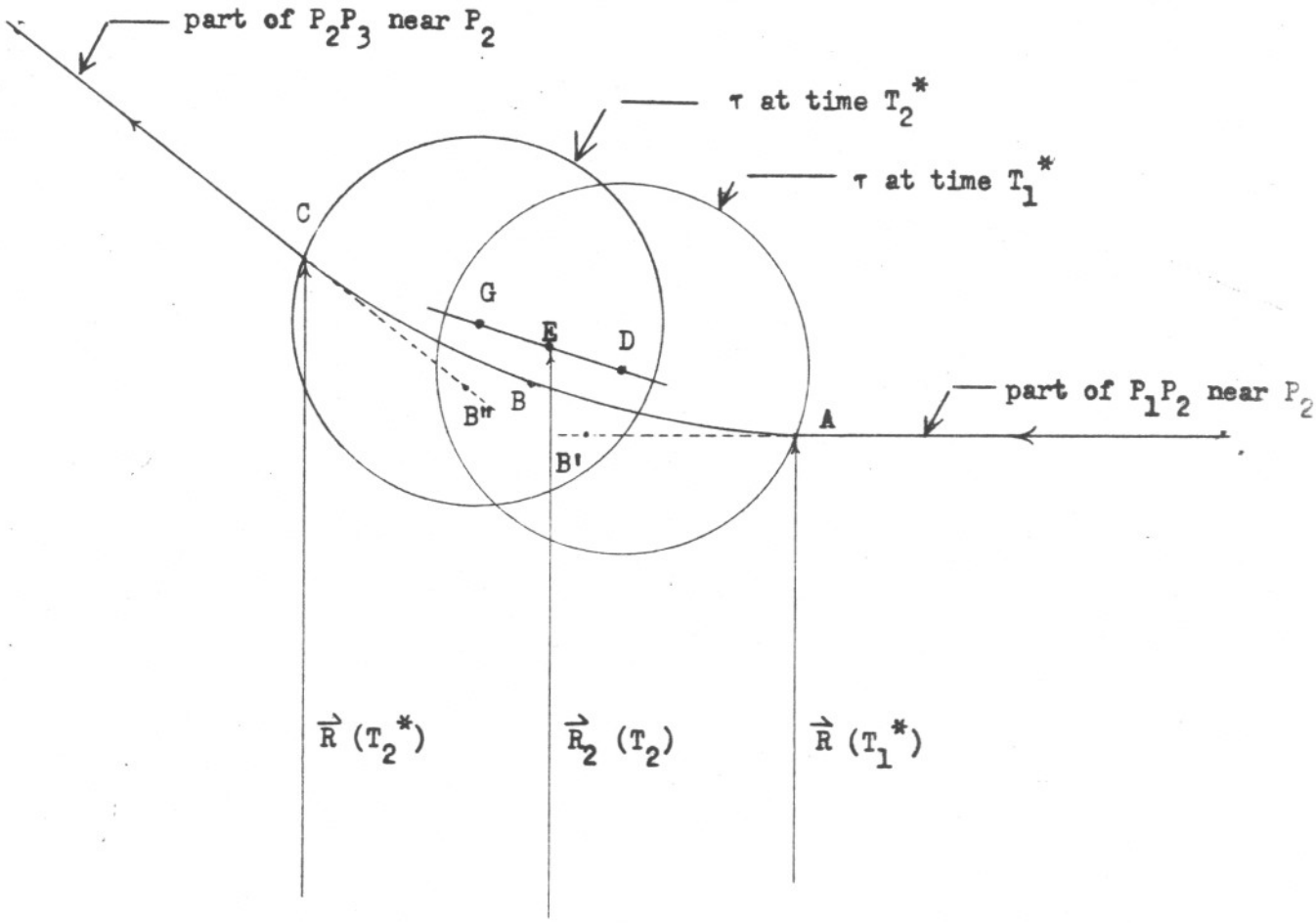

Figure 9

In the above figure the short solid line represents a small portion of P_2's orbit about the sun when the vehicle is nearby. The points D, E and G are the planets positions at T_1^*, T_2 and T_2^* respectively. The longer solid line represents a small portion of the vehicles trajectory near P_2. The point A is the position of the vehicle at the time T_1^* as it enters τ, B is its position at T_2 when it is closest to P_2 and the point C is the position of the vehicle at time T_2^* as it leaves the moving region τ. The trajectory of the vehicle bounded by A and C is not conic since the figure is drawn with respect to Σ. When viewed from Σ' this portion of the trajectory is hyperbolic. The vehicle's ellipticle trajectories outside τ appear as straight line segments because of the scale of the figure. The sun is very far away and therefore the vectors $\vec{R}(T_1^*)$, $\vec{R}_2(T_2)$ and $\vec{R}(T_2)$ appear as parallel vectors. The dotted lines are continuations of $\overset{\frown}{P_1 P_2}$ and $\overset{\frown}{P_2 P_3}$. The points B' and B" correspond to the positions of the vehicle moving on the orbits of $\overset{\frown}{P_1 P_2}$ and $\overset{\frown}{P_2 P_3}$ at the time T_2 as though P_2 did not exist. The figure clearly displays some very important facts.

It is easy to see that the position vectors of B' and B" are almost identical with $\vec{R}_2(T_2)$. Thus by employing Lambert's Theorem using the appropriate formula from (24)-(29) with $T = T_2 - T_1$, $\vec{R}_1 = \vec{R}_1(T_1)$ and $\vec{R}_2(T_2)$, the semi-major axis a_1 of $\overset{\frown}{P_1 P_2}$ can be calculated. Then by using either (32) or (33) depending upon which formula was used to calculate a_1, the eccentricity e_1 can be found. Consequently since $\ell_1 = a_1(1 - e_1^2)$ the vectors $\vec{e}_1$ and $\vec{h}_1$ corresponding to $\overset{\frown}{P_1 P_2}$ can be calculated by (8) - (12).

Similarly by setting $T = T_3 - T_2$, $\vec{R}_1 = \vec{R}_2(T_2)$ and $\vec{R}_2 = \vec{R}_3(T_3)$ an application of Lambert's Theorem yields $a_3 = a_3(T_3)$. Since T_3 is unknown a_3 is written as $a_3(T_3)$ meaning that a_3 is a function of T_3. Following the above procedure the functions $e_3(T_3)$, $\ell_3(T_3)$, $\vec{e}_3(T_3)$ and $\vec{h}_3(T_3)$ can in theory be obtained. In practice these functions are not actually determined since high speed digital computers makes it possible to give T_3 an actual trial numerical value. Thus $a_3(T_3)$, $e_3(T_3)$, $\ell_3(T_3)$, $\vec{e}_3(T_3)$ and $\vec{h}_3(T_3)$ all take on actual numerical values corresponding to the trial value given to T_3.

The actual value of T_3 can be obtained by noticing a second important fact suggested from the above figure. It is clearly evident that the vehicles velocity vector at A and C are almost identical with the hypothetical velocity vectors at B' and B". Consequently in view of our first observation these velccities can easily be obtained by (13)

$$\vec{V}(T_1^*) = \frac{1}{\ell_1} \vec{h}_1 \times (\hat{R}_2(T_2) + \vec{e}_1)$$

$$\vec{V}(T_2^*) = \frac{1}{\ell_3(T_3)} \vec{h}_3(T_3) \times \left(\hat{R}_2(T_2) + \vec{e}_3(T_3)\right)$$

Thus the actual value of T_3 is that value yielding a solution to (40). In general there are an infinite set of values of T_3 generating vectors $\vec{V}(T_2^*)$ which satisfies (40) but we shall choose that solution which gives $T_3 - T_2$ the smallest value. Thus a systematic search for T_3 can be initiated which, when found, determines the values of a_3, e_3 ℓ_3, $\vec{e}_3$, and $\vec{h}_3$ along with $\vec{V}(T_2^*)$. Hence the elliptical orbits associated with $\overset{\frown}{P_1P_2}$ and $\overset{\frown}{P_2P_3}$ can be completely determined. We emphasize at this point that even though $\vec{V}(T_1^*)$ and $\vec{V}(T_2^*)$ are known, T_1^*, T_2^*, $\vec{R}(T_1^*)$ and $\vec{R}(T_2^*)$ remain to be calculated.

C. The Determination of the Hyperbolic Trajectory

We now consider that part of the vehicles trajectory in τ. This seemingly difficult task of finding this trajectory turns out to be surprisingly easy.

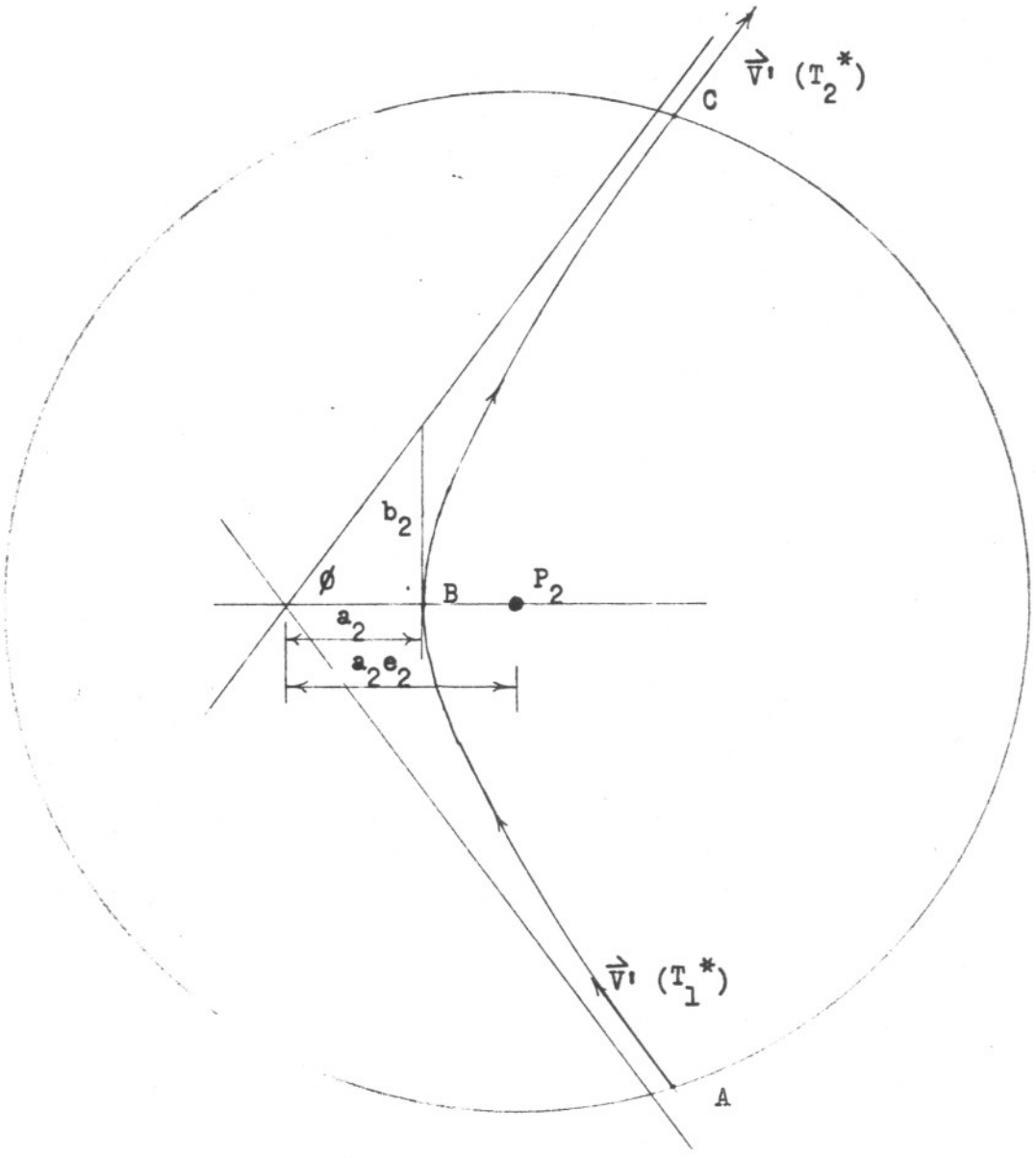

Figure 10

The above figure is drawn with respect to Σ'. Hence the vehicles trajectory in τ is hyperbolic. The points A,B and C correspond to the points A,B and C of the previous figure. From (36) we calculate the hyperbolic excess velocity vectors at A and C.

$$\vec{V}'(T_i^*) = \vec{V}(T_i^*) - \vec{V}_2 \qquad (i = 1,2)$$

The quantities $V'^2(T_1^*)$ and $V'^2(T_2^*)$ are now calculated and in view of (38) we calculate their average $\bar{V}'^2$.

$$\bar{V}'^2 = \frac{1}{2}\left(V'^2(T_1^*) + V'^2(T_2^*)\right)$$

Thus by applying the energy equation (14) we calculate the semi-major axes a_2 of the hyperbolic trajectory.

$$a_2 = \frac{u_2 \rho^*}{\bar{V}'^2 \rho^* - 2u_2} \qquad (41)$$

where

$$\rho^* = \left(\frac{m}{M}\right)^{\frac{2}{5}} R_2(T_2).$$

The term $2u_2$ is negligible compared to $\bar{V}'^2 \rho^*$ since with respect to the hyperbolic trajectory the sphere of influence lies at infinity. Hence this term may be omitted from (41) with little or no effect.

If we denote the length of the conjugate axis of the hyperbolic path by b_2 as shown in the figure one observes that

$$\tan \phi = \frac{b_2}{a_2}$$

where ϕ is one half of the angle between the asymptotes. Thus since the eccentricity e_2 is related to a_2 and b_2 by

$$e_2 = \sqrt{1 + \left(\frac{b_2}{a_2}\right)^2}$$

we obtain

$$\cos \phi = \frac{1}{e_2} \tag{42}$$

Hence by studying the figure we find

$$\vec{V}'(T_1^*) \cdot \vec{V}'(T_2^*) = V'(T_1^*)\, V'(T_2^*) \cos 2\left(\frac{\pi}{2} - \phi\right)$$

which is expressible as

$$\vec{V}'(T_1^*) \cdot \vec{V}'(T_2^*) = V'(T_1^*)\, V'(T_2^*)\,(1 - 2\cos^2 \phi)$$

Thus by making use of (42) the eccentricity of the hyperbolic path can be calculated by

$$e_2 = \left\{ \frac{2\, V'(T_1^*)\, V'(T_2^*)}{V'(T_1^*)\, V'(T_2^*) - \vec{V}'(T_1^*) \cdot \vec{V}'(T_2^*)} \right\}^{\frac{1}{2}} \tag{43}$$

The distance of closest approach to the surface of P_2 can now be easily calculated by

$$d = a_2 (e_2 - 1) - \text{Radius of } P_2 \tag{44}$$

If this quantity turns out to be negative the trajectory is obviously physically unrealizable. The value of T_3 is then progressively increased by appropriate amounts until the next smallest value of T_3 is found.

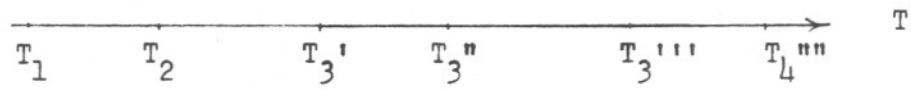

Figure 11

Figure 11 represents the general characteristic properties of all T_3 values in some interval of time after T_2. The values of T_3' and T_3'' satisfy (40) but give a negative value to the distance of closest approach. T_3''' is the next T_3 value but yields a positive distance of closest approach. This is the value we choose to take. T_3'''' is the next possible T_3 value yielding a positive value to d.

After T_3 has been determined, the velocity at closest approach V'_{CA} with respect to P_2 can be obtained by again making use of the energy equation. One easily finds

$$V'_{CA} = \sqrt{\frac{u_2}{a_2} \left(\frac{e_2 + 1}{e_2 - 1}\right)} \tag{45}$$

The magnitude of the H-vector can be calculated by

$$h_2 = \sqrt{u_2 a_2 (e_2^2 - 1)} \ . \tag{46}$$

By observing the figure on page (34) of the trajectory of the vehicle in τ with respect to Σ', the E and H vectors can readily be obtained by

$$\vec{e}_2 = \frac{\vec{V}'(T_1^*) - \vec{V}'(T_2^*)}{\left|\vec{V}'(T_1^*) - \vec{V}'(T_2^*)\right|} \ e_2 \tag{47}$$

$$\vec{h}_2 = \frac{\vec{V}'(T_1^*) \times \vec{V}'(T_2^*)}{\left|\vec{V}'(T_1^*) \times \vec{V}'(T_2^*)\right|} \quad h_2 \tag{48}$$

The position vectors of the points A and C with respect to Σ' can now be calculated by employing (4). We take as before

$$\rho(T_1^*) = \rho(T_2^*) = \rho^* = \left(\frac{m}{M}\right)^{\frac{2}{5}} \quad R_2(T_2)$$

since the radii of the spheres of influence at times T_1^* and T_2^* are almost identical with the radius at the time T_2. Consequently we have

$$\vec{\rho}(T_i^*) = \left(\frac{1}{u_2} \vec{V}'(T_i^*) \times \vec{h}_2 - \vec{e}_2\right) \rho^* \qquad (i = 1,2) \tag{49}$$

If we take ΔT to be the total amount of time the vehicle spends in τ we obtain by (35) setting $R_o = a_2(e_2 - 1)$ and $R = \rho^*$

$$\Delta T = 2\sqrt{\frac{a_2}{u_2}} \quad (\alpha - \beta) \tag{50}$$

where

$$\alpha = \sqrt{\rho^{*2} + 2 a_2 \rho^* - a_2^2 (e_2^2 - 1)}$$

$$\beta = a_2 \log \left[\frac{1}{a_2 e_2} (\alpha + \rho^* + a_2)\right]$$

Hence we may calculate T_1^* and T_2^* by

$$T_1^* = T_2 - \frac{1}{2}\Delta T$$

$$T_2^* = T_2 + \frac{1}{2}\Delta T.$$

Since T_1^* and T_2^* have been determined the position vectors of A and C can be calculated with respect to Σ by

$$\vec{R}(T_i^*) = \vec{R}_2(T_i^*) + \vec{\rho}(T_i^*) \qquad (i = 1,2) \qquad (51)$$

We have now completely determined both arriving and departing elliptical transfer trajectories and the trajectory of the vehicle near the planet P_2 which will take the vehicle to P_3. Of course in view of the above approximations the trajectory is not exact. However one may now, by an obvious iteration process, proceed to obtain a trajectory which is arbitrarily close to the desired elliptical and hyperbolic parts of the total trajectory. In practice it turns out that these approximations introduces very little error so that it is impractical to obtain greater accuracy.

We sum up this section with a very important observation. Recalling the method of solution we first determined $\overset{\frown}{P_1 P_2}$ from the given initial conditions. Then we prodeeded to find $\overset{\frown}{P_2 P_3}$ by solving (40) such that $d > 0$. Finally the trajectory in τ was calculated. Now instead of terminating the mission at P_3 suppose we wish to use P_3 to go on to some other planet say P_4. Since the initial conditions specifying T_1, T_2, P_1 and P_2 is equivalent (on an interplanetary scale) to specifying $\overset{\frown}{P_1 P_2}$ we simply take $\overset{\frown}{P_2 P_3}$ as an initial condition to proceed to P_4. Thus $\overset{\frown}{P_3 P_4}$ and the hyperbolic trajectory in the vicinity of P_3 can be determined by a completely analogous manner. Hence our method permits one to determine for more advanced and complex space trajectories. The numerical results which we take up in the next section clearly displays the feasibility of such advanced missions.

IV. Numerical Results

In Section III we were able to determine very general and complicated interplanetary free-fall trajectories. This was accomplished by employing the vector techniques developed in Section II and assuming that only one body of the solar system at any given time influences the vehicles motion. The following examples depict typical advanced free-fall interplanetary trajectories which we are concerned with:

i Trajectories of vehicles launched from earth at a given time T_1 which makes a closest approach to venus at a given time T_2 (T_2 shall continue to be called the venus intercept date) such that the gravitational influence of venus sends the vehicle back to earth (earth-venus-earth)

ii Trajectories of vehicles launched from earth at a given time T_1 which intercepts mars at a given time T_2 such that the gravitational influence of mars sends the vehicle back to earth (earth-mars-earth)

iii Trajectories of vehicles launched from earth at T_1 making a closest approach to venus at T_2 whose gravitational influence sends the vehicle on an intercept course with mercury (earth-venus-mercury)

iv Trajectories of vehicles launched from earth at T_1 making a closest approach to venus at T_2 where the gravitational influence of venus causes the vehicle to intercept mars such that the gravitational influence of mars sends the vehicle back to earth (earth-venus-mars-earth)

v Trajectories of vehicles launched from earth at T_1 making a closest approach to venus at T_2 which causes the vehicle to intercept mars which in turn causes the vehicle to return to earth where the earth's gravitational influences causes the vehicle to repeat the same flight; sending it on to venus such that venus's influence sends it to mars whereupon the martian gravitational influence causes the vehicle to return to earth (earth-venus-mars-earth-venus-mars-earth)

These examples represent only a very small fraction of the total number of possible different types of advanced interplanetary free-fall trajectories having n-1 planetary encounters. For example the total number of different types of advanced trajectories having only 2 planetary encounters of the form P_1-P_2-P_3 where P_1 = earth is 9^{3-1} or 81! In general the total number of different trajectories of the form P_1-P_2-...-P_n having n-1 planetary encounters is 9^n. Thus the trajectory given by iv

is only one of the 729 different types possible of the form P_1-P_2-P_3-P_4 where P_1 = earth.

Actual numerical calculations of even the most simplest types of these advanced trajectories having only 2 planetary encounters have (as far as the author knows) never been carried out. A few round trip trajectories to mars of the type given in example ii have been calculated at the Massachuetts Institute of Technology by R. Battin but these lacked an accurate determination of the critical hyperbolic part of the trajectories in the vicinity of mars. Battin's calculations were carried out by assuming that only the sun influences the vehicles motion during the entire mission. He assumes that the effect of mars on the total trajectory can be taken as an "impulse in velocity applied at the instant the spaceship crosses the martian orbit." This assumption is indeed very good if the word "total" is underlined. The most important part of the trajectory however, is not the transfer trajectories but the trajectory in the vicinity of mars when the vehicle is inside its gravitational sphere of influence. It is this part of the trajectory which is responsible for having the vehicle return to earth.

Battin reported on six different trajectories of which the shortest flight time was about 1050 days (see "The Determination of Round-Trip Planetary Reconnaissance Trajectories"; Journal of the Aero/Space Sciences; Sept. 1959). This minimum total flight time is obviously too long for serious consideration. Consequently as the program for the digital computer was being written corresponding to section III, many important questions remained unanswered. For example, since Battin calculated flight times in excess of 1000 days for relatively simple trajectories like ii how much time would trajectories like iv require? Moreover it was not even known whether trajectories like iii were even possible, to say nothing of trajectories like v.

When the early numerical calculations were confermed by elaborate integrating programs at the Jet Propulsion Laboratory, the Computing Facility at the University of California at Los Angeles where the program was written, began the first extensive

analytical analysis of these advanced trajectories. These early calculations at UCLA not only proved the feasibility of such missions, they showed that in some cases they would become an economic necessity.

As the numerical calculations were stepped up by also utilizing the computing complex at the Jet Propulsion Laboratory, three distinct types of advanced missions began to crystalize. These missions follow in a natural chronological order:

A. Unmanned exploration of the inner planets by instrumented space vehicles

B. Initial interplanetary missions by manned vehicles

C. Interplanetary transportation networks to support manned bases on the inner planets

We now consider each of the three types of missions separately.

A. Unmanned Exploration of the Inner Planets by Instrumented Space Vehicles on Advanced Trajectories
This category of missions utilizing advanced trajectories must simultaneously satisfy the following three important requirements:

(1) short flight times

(2) low launch energies

(3) safe distances of closest approach

In view of the first desired characteristic property these missions employing anvanced trajectories must be of the form

$$P_1 - P_2 - P_3$$

where P_1 = earth, $P_2 \neq P_3$ and must be either mercury, venus or mars. Consequently the six possibilities are:

Earth-Mercury-Venus

Earth-Mercury-Mars

Earth-Venus-Mercury

Earth-Venus-Mars

Earth-Mars-Mercury

Earth-Mars-Venus

The first two possibilities can be eliminated immediatley because launch energies for earth-mercury transfers are very high.

The last two possibilities were considered to be impractical for unmanned space probes. These trajectories shall however be studied and the results will be given at a later date. Thus only two types of missions out of the six possibilities will be considered in this paper.

a. Earth-Venus-Mercury

b. Earth-Venus-Mars

The analysis proceeded by first noting that any favorable launch period requiring low launch energies and relatively short flight times for these advanced trajectories will also be a favorable launch period for simple direct flight trajectories to venus. In general any favorable launch period for any advanced free-fall interplanetary trajectory of the form P_1-P_2-...-P_n where P_1 = earth and P_2 = venus will necessarily be a favorable launch period for simple earth-venus trajectories. The converse of course is obviously false. In view of this simple but important observation, a great number of these advanced trajectories were not calculated because if a launch date did not fall in some favorable earth-venus launch period the advanced trajectory would automatically require a high launch energy. These favorable earth-venus launch periods were all found by preliminary calculations utilizing Lambert's Theorem.

For each launch date (differing by 2 day increments and running continuously through the entire decade) a large set of simple earth-venus transfer trajectories were calculated corresponding to various flight times. Letting θ_{12} denote the heliocentric angle associated with each trajectory, we partitioned each set into three subsets characterized by $0^\circ < \theta_{12} < 180^\circ$, $180^\circ < \theta_{12} < 360^\circ$ and $360^\circ < \theta_{12} < 540^\circ$. The trajectories of each subset are called Type I, Type II and Type III respectively. By the optimum Type I, Type II and Type III trajectories for a particular launch date T_1 we shall mean the trajectories having least launch energy from among those trajectories in each of the three subsets of the set corresponding to the launch date T_1. For some launch dates these optimum trajectories have relatively low launch

energies. These periods of relatively low launch energies are the favorable launch periods. The favorable periods for Type I and Type II trajectories almost always coinsides with each other but the favorable periods for Type III trajectories are quite distinct from the other two. Type III trajectories require longer flight times than those of Type I or Type II. Consequently we shall restrict the P_1-P_2 transfer trajectories to be either Type I or Type II.

In Table 1 all the favorable Type I and Type II earth-venus launch periods occuring in the 10 year time interval beginning with 1965 and running through 1974 are given. We observe that there are only six such periods for the decade. Each period was chosen to be approximately two months long. Notice that the middle of successive periods are separated by about 19.2 months. As one might suspect this is approximately venus's synodic period. The table also gives some important properties of the optimum trajectories associated with each period. The symbols HEV_1 and HEV_2 denote the vehicles hyperbolic excess velocity (in km/sec) as it leaves the first planet (earth) and as it arrives at the second planet (venus) respectively. A vehicle's hyperbolic excess velocity at a planet is the amount by which the vehicle's velocity exceeds the planet's excape velocity. The flight time (in days) is denoted by T_{12}. In describing the launch or approach energies w we shall refere to the vis-viva energies which are the squares of the hyperbolic excess velocities; they shall always be ommitted. For example from Table 1 we observe that the lowest launch energy required for Type I trajectories of the 1965 period is 1.84 times greater than the lowest launch energy for Type II trajectories of the same launch period.

In order that the full potentialities of the advanced trajectories corresponding to a and b be clearly understood, let us examine the optimum earth-mercury and earth-mars trajectories for their respective favorable launch periods during the 1965-1974 time interval. Calculations of optimum earth-mercury and earth-mars transfer trajectories were carried out like those for the earth-venus trajectories.

TABLE 1

Some Important Properties of Optimum Earth-Venus Transfer Trajectories

TYPE I

Launch Period	Min HEV_1	Max HEV_1	Min T_{12}	Max T_{12}	Min HEV_2	Max HEV_2
10/17/65 - 12/4/65	3.65	4.25	104	122	2.90	6.23
5/10/67 - 7/11/67	2.52	4.22	118	144	2.86	5.81
12/10/68 - 2/6/69	2.77	3.59	106	154	3.78	4.58
7/13/70 - 9/11/70	2.91	3.64	96	144	5.04	5.75
2/21/72 - 4/21/72	3.50	4.42	94	136	5.02	7.21
10/13/73 - 12/6/73	3.65	4.40	102	122	2.91	6.44

TYPE II

Launch Period	Min HEV_1	Max HEV_1	Min T_{12}	Max T_{12}	Min HEV_2	Max HEV_2
6/21/65 - 8/26/65	2.69	3.66	134	184	4.12	4.46
4/24/67 - 6/15/67	2.41	3.28	148	184	2.86	4.43
1/9/69 - 3/10/69	3.54	3.74	168	178	4.43	7.82
8/14/70 - 10/11/70	3.00	3.57	160	178	5.28	7.25
3/6/72 - 5/5/72	2.86	3.44	164	186	4.86	6.59
10/5/73 - 12/4/73	2.71	3.54	136	178	4.15	5.14

TABLE 2

Some Important Properties of Optimum Earth-Mercury Transfer Trajectories

TYPE I

Launch Period	Min HEV_1	Max HEV_1	Min T_{12}	Max T_{12}	Min HEV_2	Max HEV_2
1/1/65 - 2/3/65	7.20	7.88	86	114	15.42	18.32
12/6/65 - 1/17/66	6.84	7.82	86	122	15.57	18.04
11/15/66 - 12/31/66	6.59	7.91	86	126	15.50	17.05
11/10/67 - 12/12/67	6.46	7.78	88	116	14.19	15.35
11/6/68 - 11/24/68	6.85	7.92	92	104	12.48	16.24
2/15/70 - 3/1/70	8.01	8.14	88	100	14.65	15.78
1/19/71 - 2/14/71	7.50	7.94	86	108	16.00	17.07
12/21/71 - 1/28/72	7.04	7.93	84	116	16.14	18.96
11/25/72 - 1/10/73	6.72	7.88	84	126	16.13	17.59
11/12/73 - 12/22/73	6.49	7.73	88	124	14.85	15.99
11/9/74 - 12/5/74	6.43	7.87	90	110	12.15	15.36

TYPE II

Launch Period	Min HEV_1	Max HEV_1	Min T_{12}	Max T_{12}	Min HEV_2	Max HEV_2
8/28/65 - 9/19/65	7.50	7.87	108	124	12.98	14.40
8/17/66 - 9/4/66	7.98	8.20	108	120	13.05	15.06
11/3/66 - 11/13/66	8.09	8.26	134	142	12.15	14.61
10/19/67 - 11/22/67	6.94	7.94	120	142	11.94	14.64
10/3/68 - 11/18/68	6.44	7.95	108	142	12.00	16.25
9/22/69 - 11/5/69	6.56	7.84	98	138	12.21	13.15
9/11/70 - 10/21/70	6.85	7.69	104	134	12.96	14.70
9/2/71 - 10/2/71	7.23	7.86	106	128	12.95	14.63
8/25/72 - 9/12/72	7.70	7.93	108	122	13.35	14.57
10/29/73 - 11/18/73	7.57	7.94	130	140	12.02	13.47
10/12/74 - 11/21/74	6.62	7.94	116	144	11.82	14.67

TABLE 3

Some Important Properties of Optimum Earth-Mars Transfer Trajectories

TYPE I

Launch Period	Min HEV_1	Max HEV_1	Min T_{12}	Max T_{12}	Min HEV_2	Max HEV_2
12/5/66 - 2/3/67	3.00	4.23	190	208	4.05	6.89
2/2/69 - 4/3/69	2.96	3.84	176	214	3.60	6.52
4/23/71 - 6/22/71	2.81	3.52	188	228	2.80	3.61
7/7/73 - 8/16/73	3.80	4.25	194	198	2.55	3.44

TYPE II

Launch Period	Min HEV_1	Max HEV_1	Min T_{12}	Max T_{12}	Min HEV_2	Max HEV_2
12/21/66 - 2/19/67	2.94	3.00	308	348	3.63	6.35
2/26/69 - 3/27/69	2.82	3.02	288	302	4.53	5.41
4/9/71 - 5/31/71	3.09	4.00	244	296	3.10	3.76
8/4/73 - 9/11/73	4.00	4.20	364	442	3.13	4.22

Tables 2 and 3 give their respective periods along with some important facts similar to table 1. Since Mercury's synodic period is approximately $\frac{1}{5}$ th. venus's there are about 5 times as many relative minimum launch energy periods. Unlike the earth-venus periods, the minimum launch energy for each period for the earth-mercury trajectories sometimes vary by more than 200%. This is due to mercury's high eccentricity and inclination to the ecliptic. Consequently only 11 earth-mercury launch periods appear in Table 2. These are the 11 most favorable periods.

The synodic period of venus is approximately $\frac{3}{4}$ 'ths. as long as the synodic period for mars. Thus since there are 6 earth-venus periods for the decade there should be only $4\frac{1}{2}$ earth-mars periods. The beginning of the decade falls almost in the middle of an earth-mars period. This accounts for the expected half period. Table 3 displays the 4 complete earth-mars launch periods.

It is important to keep in mind that the trajectories described in the three tables are optimum trajectories. Thus from Table 1 we notice that the lowest hyperbolic excess velocity required to reach venus on a Type I trajectory for the entire decade is 2.52 km/sec and occures during the 1967 launch period. Only 2.41 km/sec is required for a Type II trajectory which also occures during the 1967 period. From Table 2 we find that the lowest hyperbolic excess velocity required to reach mercury during the decade is 6.43 km/sec. The required trajectory is Type I and occures during the 1974 launch period. This minimum energy is 267% greater than the lowest launch energy required to reach venus. The lowest hyperbolic excess velocity required to reach mars during the decade is 2.81 km/sec.

The information given in the tables clearly displays the following hard facts:

(1) Launch energies for direct earth-mercury trajectories are very high.

(2) There are relatively few launch opportunities for direct earth-mars missions; each are separated by approximately 780 days.

We shall now see that the barrier obstructing trips to mercury can be circumvented by replacing the earth-mercury trajectories by the earth-venus-mercury trajectories and the 4 available launch periods for trips to mars can be increased to 7 by utilizing earth-venus-mars trajectories.

a. Earth-Venus-Mercury trajectories

We recall that any advanced trajectory having P_1 = earth and P_2 = venus will necessarily require a high launch energy if the launch date does not fall in one of the favorable earth-venus launch periods. Consequently the numerical analysis of the earth-venus-mercury trajectories proceeded by first carrying out a rough analysis over each of the six earth-venus launch periods given in Table 1. These calculations were aimed at finding the approximate values of the pairs (T_1, T_2) which yielded the most promising trajectories for each period. This involved determining many trajectories with initial conditions (T_1, T_2) represented by the intersections in a net about each launch period. We shall refer to these nets as the coarse nets. For example the coarse net about the 1965 launch period is shown by figure 12.

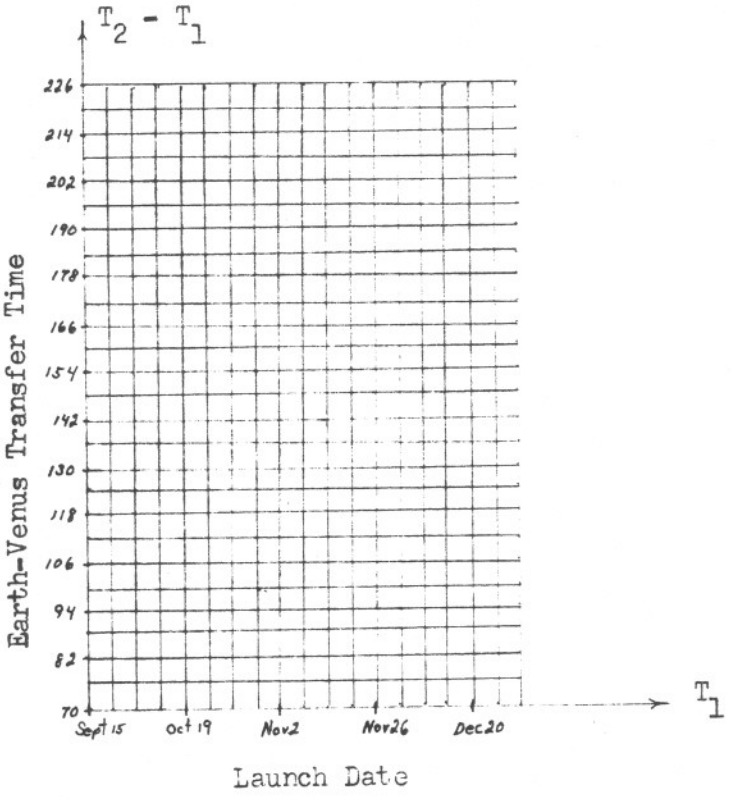

Figure 12

Notice that this launch interval and its range of flight times completely covers the 1965 earth-venus launch period given in table 1.

The calculation of this net was performed by first setting T_1 = Sept. 15, 1965 and T_2-T_1 = 70 days. After this trajectory was calculated (or rejected bacause its flight time was too long or because it was physically unrealizeable) the next trajectory having the same launch date but with T_2-T_1 = 76 days was calculated (or rejected). This proceeded until the earth-venus flight time (T_2-T_1) reached 226 days whereupon the launch date was advanced 6 days to Sept. 21 and T_2-T_1 dropped back to 70 days. This was done until the 19 different launch dates were exhausted. This involved the calculation of 27x19=513 trajectories for each of the two types of missions. The grid of this net will be referred to as 6 days by 6 days where the first number means that the venus intercept date was advanced by 6 day intervals for each fixed launch date and the second number means that the launch dates were advanced by 6 day intervals. This grid was used for all coarse nets except for the 1967 period. In this case a 1 by 4 day grid was employed.

These coarse net results revealed that all six earth-venus launch periods were also periods for possible earth-venus-mercury missions. Thus it was discovered that these trajectories were not only possible but even occured during each earth-venus period throughout the entire decade.

Guided by the results of the coarse nets a much more localized study was begun. For each period this involved calculating a much finer net covering the most attractive trajectories found by the coarse net. These fine nets employed a grid of .2 by 2 days. Thus corresponding to each launch date of the fine net as many as 250 different trajectories were sometimes determined. Consequently in some fine nets almost 5000 advanced trajectories were calculated (of which many were rejected). It was observed that advancing the venus intercept date by only .2 day increments sometimes produced a 200-500 km change in the distance of closest approach. Thus when the distance of closest approach became small for some launch periods a third extra fine net employing a grid of .01 by 2 days was calculated. From the results of all these calculations the trajectories having either the lowest launch energy or the maximum distance of closest approach for each launch date of a net were found.

All the tables appearing in this paper shall adhere to the following notation.

HEV_k = hyperbolic excess velocity (km/sec) at P_k

$T_{k,k+1}$ = time taken by vehicle to pass from P_k to P_{k+1} (i.e., $T_{k+1} - T_k$)

$\theta_{k,k+1}$ = heliocentric angle swept out by the vehicle passing from P_k to P_{k+1}

$TISI_k$ = amount of time (days) vehicle spends in P_k's sphere of gravitational influence

$DCCA_k$ = distance of closest approach (km) to P_k's surface

$VACA_k$ = velocity at closest approach (km/sec) to P_k

DA_k = angular difference between the vehicle's velocity vectors as it enters and leaves P_k's sphere of influence

TFT = total flight time (days)

The quantities labled $(\vec{B} \cdot \hat{T})_k$ and $(\vec{B} \cdot \hat{R})_k$ are used by an integrating program at the Jet Propulsion Laboratory which enables the actual trajectory to be precisely determined. The vectors $\vec{B}$, $\hat{T}$ and $\hat{R}$ are defined with respect to Σ' at P_k which is taken to be an ecliptic coordinate system (ephoc 1950.0). The $\vec{B}$ vector is the vector which meets the vehicles incoming hyperbolic asymptote at right angles (km). The unit vectors $\hat{T}$ and $\hat{R}$ are defined by

$$\hat{T} = \frac{\vec{V}'(T^*_{k-1}) \times \hat{k}}{\left|\vec{V}'(T^*_{k-1}) \times \hat{k}\right|}$$

$$\hat{R} = \frac{\vec{V}'(T^*_{k-1}) \times \hat{T}}{V'(T^*_{k-1})}$$

where according to the notation of Section III, T^*_{k-1} is the time when the vehicle enters the gravitational sphere of influence of P_k.

The following comments should be carefully noted. They shall apply to all the tables given in this paper.

If some symbols do not have any subscripts the subscript k shall be assumed to be 2. For example DOCA means $DOCA_2$ etc.

The time corresponding to all given calender dates which appear without any reference to a particular time shall always be taken as 1200 hours GMT.

The radius of the planet venus which is taken to be 6100 km was determined optically (see reference 7). Consequently the distances of closest approach to venus appearing in some of the tables should be understood to mean the distances of closest approach to venus's visible cloud layer as viewed from the earth.

Earth-Venus-Mercury 1965-6

The first earth-venus launch period for the decade under consideration occures during the winter of 1965. Although accurate planetary approach guidance may not be available for this launch period it may be possible to place a vehicle on an earth-venus-mercury trajectory by employing advanced techniques of midcourse corrections. Even if the midcourse corrections were only partially successful the vehicle could perhaps obtain very useful information about regions close to the sun.

Since detailed properties of venus's atmosphere may still be unknown at this time, the trajectories appearing in table 4 were chosen so that their distances of closest approach exceeds 800 km while at the same time their launch energies are nearly minimum for each launch date of the period. These were found from the fine net results. Comparing these trajectories with the general properties of optimum earth-mercury trajectories we find some very significant characteristics. These trajectories require less than $\frac{1}{3}$ of the launch energies required for the optimum earth-mercury trajectories for the periods occuring in 1965 and 1966. We also notice that the mercury approach energies are less than $\frac{1}{2}$ of those resulting from the more simpler direct flight trajectories. Planetary approach energies will become increasingly important when orbiting or landings on the planet become necessary.

The flight times required for these advanced missions are considerably longer than those required for the more simpler trajectories but they are quite within reason. Turning to Table 3 we notice that these flight times are in the same range of flight times required for direct earth-mars missions.

It is interesting to observe the strong influence which the gravitational field of venus exerts on the vehicle's trajectory. During the 2 days when the vehicle's motion is dominated by venus's gravitational field, the direction of the

vehicle's velocity vector is altered by as much as 55°.

Before considering these trajectories for the next launch period it is desireable to have some general idea of the configuration of the planets during the critical phases of the missions when the vehicle encounters venus and mercury. This configuration is shown in figure 13. From the geometry of the situation we find that the communication distances during the venus and mercury encounters will be approximately 1.6 and 1.3 A.U. respectively. The figure reveals that special consideration must be given to radio disturbance due to the sun during the mercury encounter. This problem could be alleviated by utilizing large radio antennas with high resolution such as the new 210 ft. dish planned for the Goldstone site. Figure 14 gives part of the Dec. 18 trajectory in the sphere of influence of venus. The trajectory is drawn with respect to venus and hence is hyperbolic. According to the scale of the figure the sphere of influence has a radius of approximately 13 feet. The circle representing venus is its cloud layer and not its surface.

We have noticed that these advanced trajectories have only a fraction of the launch energies and arrival energies characteristic of the optimum earth-mercury trajectories. Besides this great saving of energy these advanced trajectories can be used not only to reach mercury but also to enable the vehicle to perform various tasks as it passes venus. For example the launch vehicle could carry two scientific payloads, one of which could be "dropped off" as it passes venus on its way to mercury. Of course vehicles capable of carrying out these sophisticated missions will weigh more than those required for direct earth-mercury flights but the proportional difference in weight should be more than off set by the lower launch energies required for these advanced trajectories.

TABLE ✱ TABLE 4

EARTH-VENUS-MERCURY

1965-6

LAUNCH DATE	HEV_1	T_{12}	θ_{12}	$\vec{B}\cdot\vec{T}$	$\vec{B}\cdot\vec{R}$	HEV_2	TISI	DOCA	VACA	DA	T_{23}	θ_{23}	HEV_3	TT
Nov. 28	4.39	186.9	264.93	-12810.	123.	7.15	1.94	1849.	11.53	52.72	110.98	241.11	9.13	297.92
30	4.32	185.3	263.55	-12845.	124.	7.10	1.95	1832.	11.50	53.22	110.25	239.41	9.18	295.59
Dec. 2	4.25	183.75	262.16	-12863.	158.	7.06	1.96	1805.	11.49	53.71	109.60	238.12	9.18	293.35
4	4.19	182.15	260.77	-12869.	108.	7.02	1.97	1772.	11.48	54.18	108.82	236.05	9.28	290.91
6	4.13	180.55	259.38	-12862.	50.	6.99	1.98	1733.	11.48	54.63	107.92	233.98	9.40	288.47
8	4.09	178.96	257.99	-12842.	-15.	6.97	1.99	1688.	11.49	55.06	107.09	231.93	9.55	286.05
10	4.05	177.36	256.60	-12807.	-91.	6.95	1.99	1637.	11.50	55.45	106.26	229.86	9.71	283.62
12	4.01	175.56	254.89	-12843.	36.	6.91	2.00	1635.	11.48	55.76	106.15	229.83	9.69	281.71
14	3.99	173.76	253.18	-12857.	132.	6.89	2.01	1622.	11.47	56.05	105.95	229.53	9.70	279.71
16	3.97	171.97	251.47	-12848.	186.	6.87	2.01	1596.	11.47	56.32	105.65	228.87	9.75	277.61
18	3.97	170.17	249.76	-12820.	205.	6.86	2.01	1560.	11.48	56.57	105.62	227.95	9.83	275.43
20	3.97	168.17	247.73	-12833.	397.	6.84	2.02	1557.	11.47	56.76	105.47	228.66	9.75	273.65
22	4.00	166.17	245.70	-12817.	547.	6.83	2.02	1538.	11.48	56.92	105.59	229.04	9.71	271.76
24	4.03	165.38	245.57	-12443.	-358.	6.91	2.00	1288.	11.65	57.25	102.31	220.06	10.76	267.69
26	4.07	164.78	245.75	-11927.	-1204.	7.01	1.97	979.	11.87	57.75	99.49	212.80	11.86	264.27
28	4.12	162.98	244.04	-11830.	-1256.	7.03	1.97	920.	11.91	57.83	99.10	211.78	12.03	262.08
30	4.19	160.98	242.01	-11787.	-1203.	7.05	1.96	893.	11.94	57.80	99.02	211.51	12.09	260.00
Jan. 1	4.27	258.98	239.98	-11718.	-1173.	7.07	1.96	855.	11.98	57.74	98.91	211.10	12.18	257.89
3	4.37	156.79	237.64	-11686.	-1047.	7.10	1.95	840.	12.00	57.58	99.08	211.32	12.18	255.87
5	4.49	154.59	235.29	-11621.	-945.	7.13	1.94	810.	12.04	57.39	99.20	211.37	12.21	253.79

Planetary Configuration For Earth-Venus-Mercury 1965-6
(Dec. 18 Trajectory)

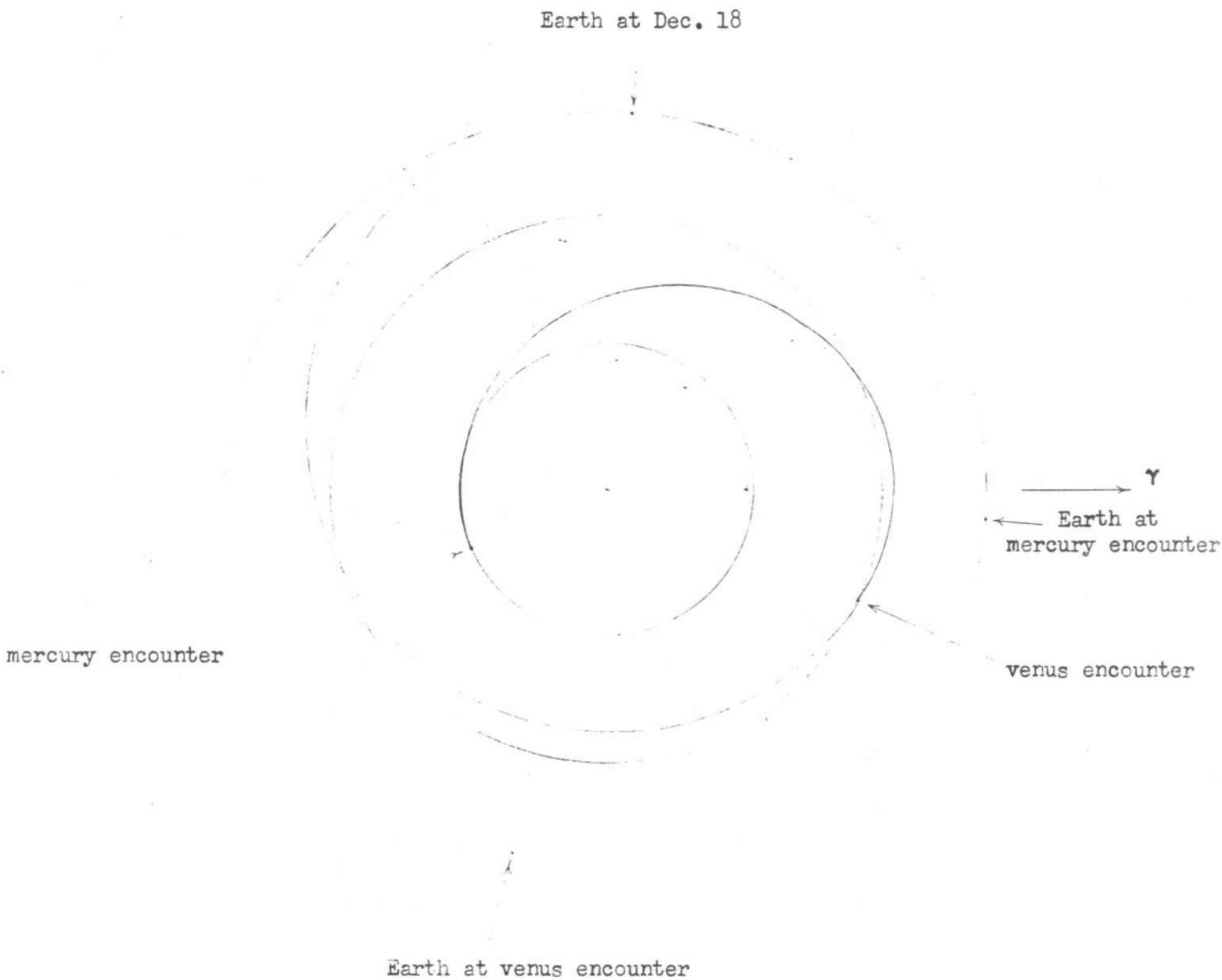

Figure 13

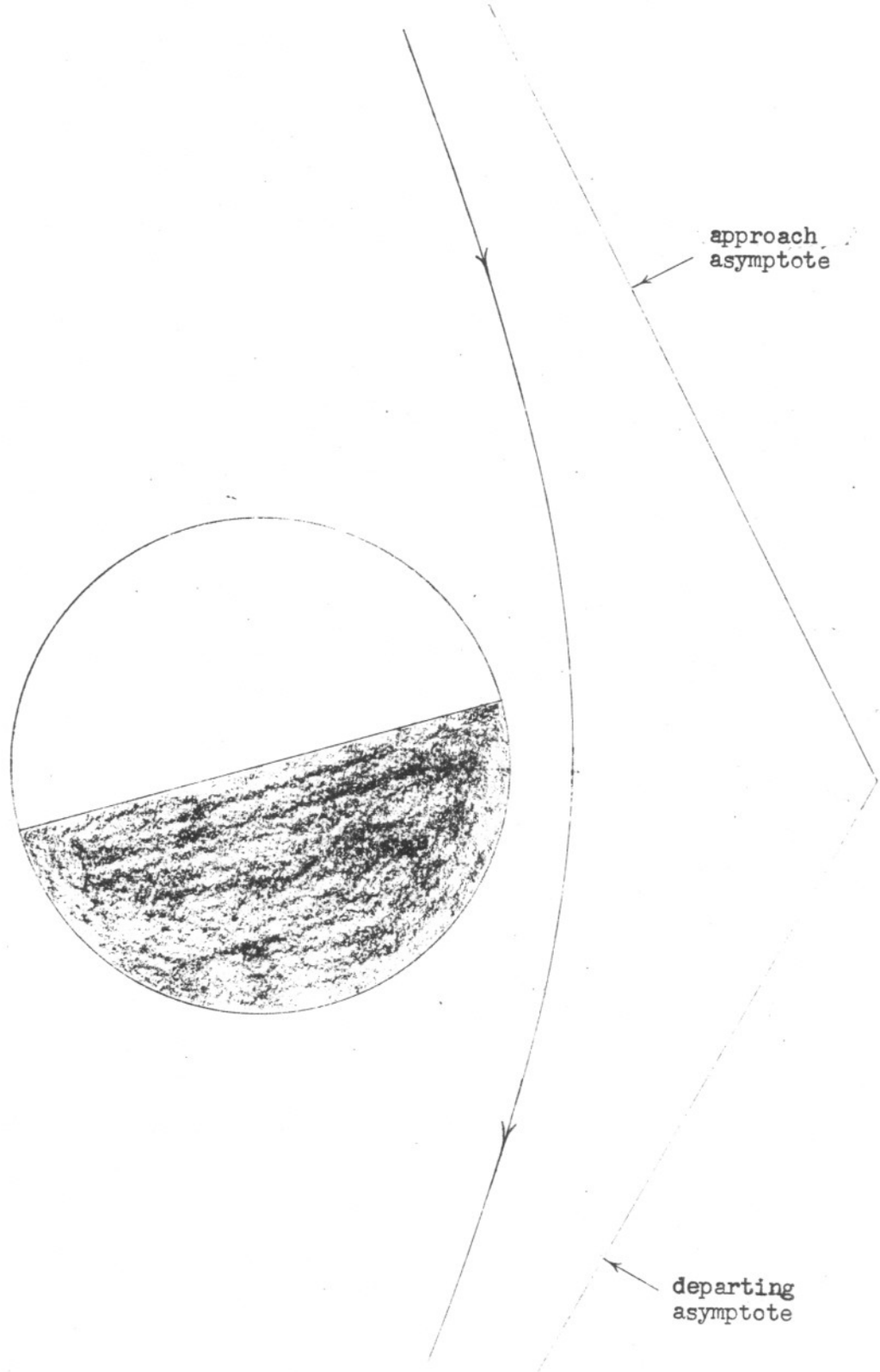

Figure 14

Earth-Venus-Mercury 1967

From table 1 we notice that the second earth-venus launch period occures during the summer of 1967. The advanced trajectories for this period come very close to venus. Consequently an extra fine net was calculated to find those trajectories corresponding to the different launch dates which maximized the distance of closest approach. Table 5 is an example of how these greatest passing distance trajectories were found. In particular it is a set of trajectories for the June 7 launch date. Each trajectory was obtained by advancing the venus intercept date T_2 by only .01 day increments. The extra fine net calculates these sets for every launch date of the period. Of course trajectories for this launch date passing much farther probably exists but they will have flight times or launch energies several times greater. Thus it shall always be assumed that maximum passing distance trajectories or minimum launch energy trajectories are referred to only those trajectories having short flight times and lowest possible launch energies.

The maximum passing distance trajectories for the various launch dates of the 1967 launch period appear in Table 6. If measurements of the venusian atmosphere show that the density at various altitudes is approximately twice as great as the densities for the earth these trajectories would be very questionable. On the other hand if the density at various altitudes is approximately equal for both planets, these trajectories may in fact be ideal. A vehicle passing just outside venus's atmosphere on its way to mercury could easily obtain excellent observations and measurements. Since these trajectories pass venus on the sunny side they would enable the vehicle to obtain very good spectroscopic measurements of its atmosphere. Moreover, equiped with an ordinary camera, the vehicle may even obtain pictures of its surface.

Table 5

SOME IMPORTANT PROPERTIES OF EARTH-VENUS-MERCURY TRAJECTORIES

(June 7, 1967 Launch)

Launch Date	HEV_1	T_{12}	θ_{12}	$\vec{B}\cdot\vec{T}$	$\vec{B}\cdot\vec{R}$	HEV_2	TISI	DOCA	VACA	DA	T_{23}	θ_{23}	HEV_3	TFT
June 7	3.56	107.32	117.77	11429.	-1524.	6.44	2.13	6.7	12.16	68.37	71.70	189.38	9.82	179.02
"	3.56	107.33	117.79	11448.	-1482.	6.44	2.13	15.8	12.15	68.34	71.71	189.44	9.80	179.04
"	3.56	107.34	117.80	11468.	-1437.	6.44	2.13	25.2	12.14	68.31	71.72	189.51	9.78	179.07
"	3.56	107.35	117.82	11487.	-1390.	6.43	2.13	34.5	12.14	68.28	71.74	189.58	9.75	179.09
"	3.56	107.36	117.83	11507.	-1343.	6.43	2.13	43.9	12.13	68.25	71.76	189.65	9.73	179.12
"	3.56	107.37	117.85	11526.	-1294.	6.43	2.13	53.1	12.12	68.21	71.77	189.73	9.70	179.15
"	3.56	107.38	117.87	11546.	-1243.	6.43	2.13	62.4	12.11	68.18	71.79	189.81	9.67	179.17
"	3.56	107.39	117.88	11565.	-1189.	6.43	2.13	71.8	12.11	68.15	71.81	189.89	9.65	179.21
"	3.56	107.40	117.90	11585.	-1134.	6.42	2.13	81.3	12.10	68.12	71.83	189.99	9.62	179.24
"	3.56	107.41	117.91	11604.	-1075.	6.42	2.13	90.9	12.09	68.09	71.86	190.09	9.59	179.27
"	3.56	107.42	117.93	11623.	-1015.	6.42	2.13	100.2	12.08	68.05	71.89	190.19	9.56	179.31
"	3.56	107.43	117.94	11643.	-951.	6.42	2.13	109.7	12.07	68.02	71.91	190.30	9.53	179.35
"	3.56	107.44	117.96	11662.	-883.	6.42	2.13	119.2	12.07	67.99	71.95	190.43	9.49	179.39
"	3.56	107.45	117.97	11681.	-812.	6.42	2.13	128.6	12.06	67.96	71.98	190.56	9.46	179.43
"	3.56	107.46	117.99	11694.	-766.	6.41	2.13	135.4	12.05	67.93	72.00	190.64	9.44	179.46
"	3.56	107.47	118.01	11717.	-644.	6.41	2.14	146.5	12.05	67.90	72.06	190.85	9.39	179.53
"	3.55	107.48	118.02	11733.	-588.	6.41	2.14	155.1	12.04	67.87	72.10	191.00	9.35	179.58
"	3.55	107.49	118.04	11754.	-477.	6.41	2.14	165.8	12.03	67.83	72.16	191.24	9.30	179.65
"	3.55	107.50	118.05	11770.	-380.	6.41	2.14	174.4	12.02	67.80	72.23	191.46	9.25	179.72
"	3.55	107.51	118.07	11787.	-261.	6.40	2.14	183.4	12.02	67.77	72.30	191.74	9.20	179.81
"	3.55	107.52	118.08	11802.	-111.	6.40	2.14	192.5	12.01	67.75	72.41	192.11	9.13	179.93
"	3.55	107.53	118.10	11815.	86.	6.40	2.14	200.9	12.00	67.72	72.57	192.65	9.05	180.10
"	3.55	107.54	118.11	11762.	967.	6.40	2.14	187.5	12.01	67.81	73.53	195.83	8.69	181.07
"	3.55	107.56	118.15	11618.	1546.	6.39	2.14	115.6	12.06	68.25	74.52	198.97	8.50	182.08
"	3.55	107.57	118.16	11541.	1761.	6.39	2.14	76.7	12.08	68.47	75.00	200.51	8.46	182.57
"	3.55	107.58	118.18	11457.	1949.	6.39	2.14	31.0	12.17	68.74	75.50	202.10	8.45	183.08

TABLE 6

EARTH-VENUS-MERCURY

1967

LAUNCH DATE	HEV_1	T_{12}	θ_{12}	$\vec{B}\cdot\vec{T}$	$\vec{B}\cdot\vec{R}$	HEV_2	TISI	DOCA	VACA	DA	T_{23}	θ_{23}	HEV_3	TFT
June 5	3.56	109.40	119.81	11812.	212.	6.37	2.15	170.	12.01	68.18	72.87	193.42	8.96	182.27
7	3.55	107.53	118.10	11815.	86.	6.40	2.14	201.	12.00	67.72	72.57	192.65	9.05	180.10
9	3.55	105.67	116.41	11816.	453.	6.42	2.13	234.	11.99	67.29	72.71	193.35	8.92	178.38
11	3.56	103.80	114.71	11816.	361.	6.45	2.12	260.	11.99	66.88	72.43	192.65	8.99	176.23
13	3.58	101.92	112.99	11808.	49.	6.48	2.12	280.	11.99	66.47	72.00	191.44	9.15	173.92
15	3.61	100.05	111.29	11793.	278.	6.50	2.11	296.	11.99	66.14	72.00	191.66	9.08	172.05
17	3.65	98.16	109.57	11774.	158.	6.53	2.10	307.	12.00	65.80	71.74	191.02	9.16	169.91
19	3.70	96.28	107.84	11745.	10.	6.56	2.09	311.	12.01	65.49	71.49	190.36	9.25	167.77
21	3.77	94.39	106.12	11709.	-22.	6.58	2.08	309.	12.03	65.22	71.32	189.99	9.30	165.71
23	3.84	92.52	104.41	11668.	4.	6.61	2.08	301.	12.05	65.00	71.18	189.74	9.31	163.69
25	3.93	90.63	102.69	11617.	-45.	6.64	2.07	286.	12.07	64.80	71.00	189.35	9.36	161.63
27	4.04	88.73	100.95	11552.	-147.	6.67	2.06	262.	12.11	64.64	70.81	188.91	9.44	159.55
29	4.16	86.85	99.22	11480.	-189.	6.69	2.05	230.	12.14	64.52	70.66	188.58	9.48	157.50
July 1	4.29	84.96	97.51	11399.	-195.	6.72	2.04	189.	12.18	64.46	70.52	188.31	9.51	155.48
3	4.44	83.08	95.78	11304.	-245.	6.75	2.04	139.	12.23	64.44	70.36	187.99	9.56	153.44

Planetary Configuration For Earth-Venus-Mercury 1967
(June 19 Trajectory)

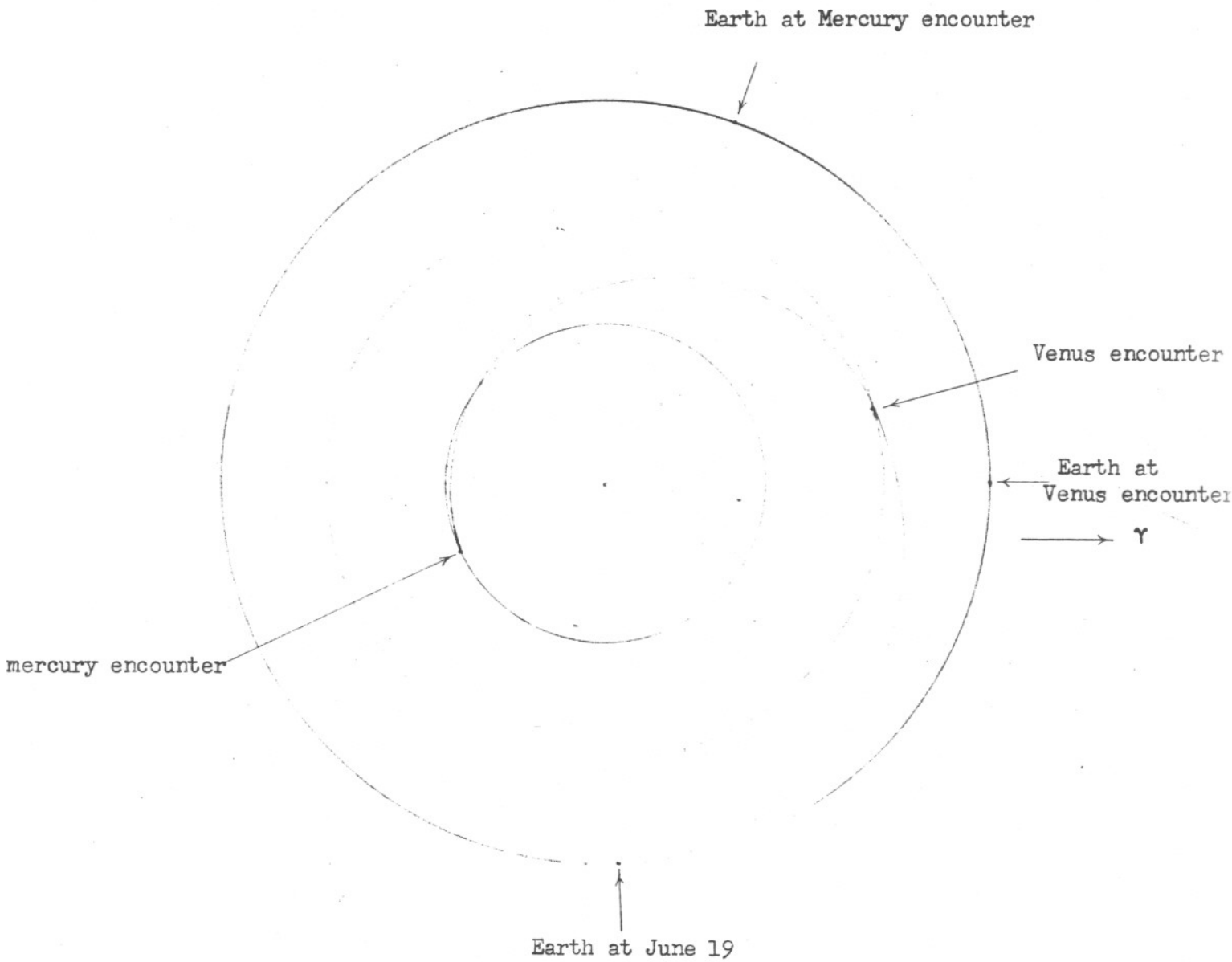

Figure 15

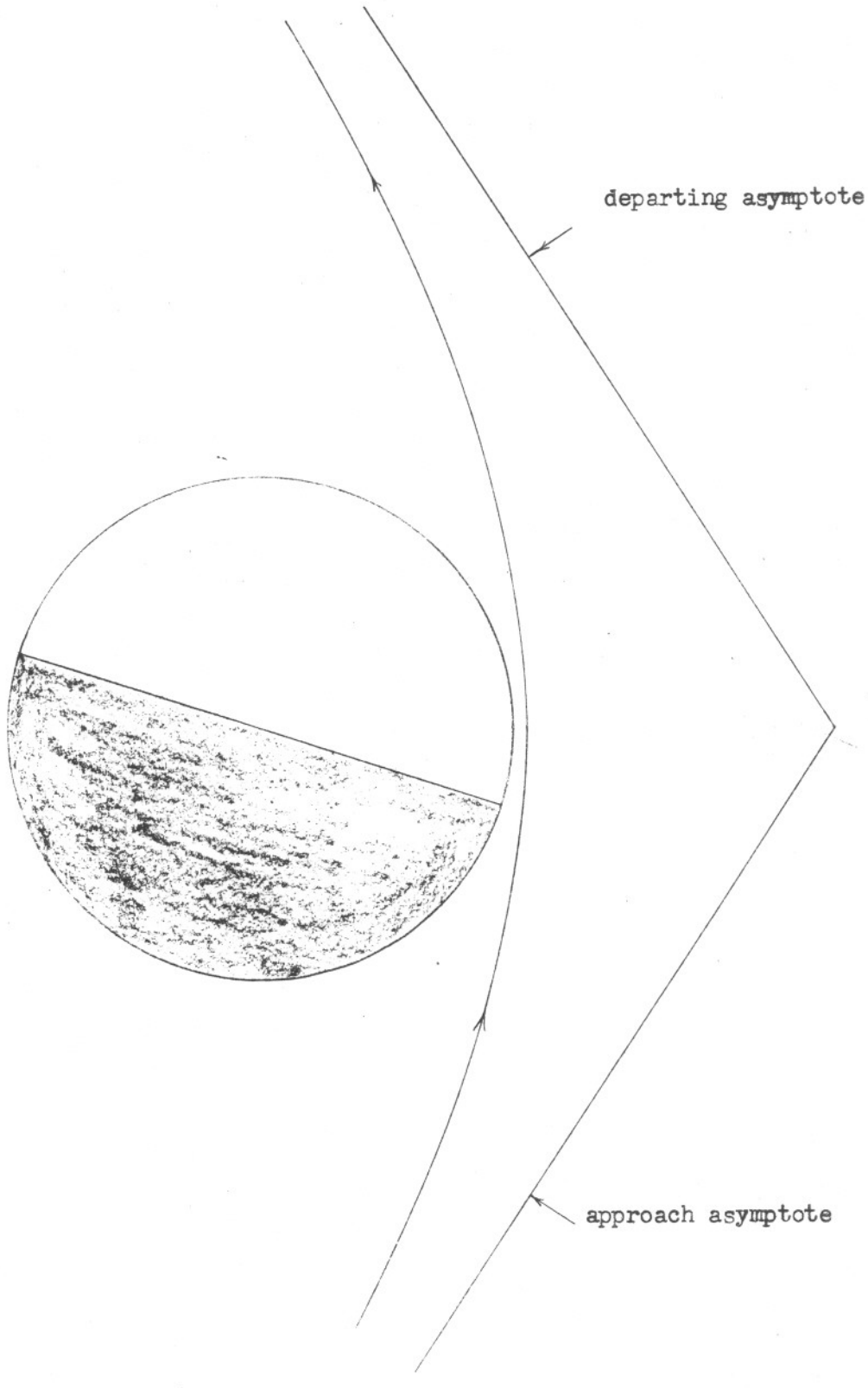

Figure 16

Unlike the trajectories for the 1965-6 launch period these trajectories take the vehicle less than half way around the sun for the earth-venus legs of the mission. The transfers to mercury are also shorter. Thus these trajectories have flight times approximately 100 days shorter than those of the previous launch interval. Notice that the launch energies are lower than those for the 1965-6 launch period. The mercury approach energies are also lower. One observes that a vehicle moving on these trajectories spends slightly more time under the gravitational influence of venus. This together with the fact that these trajectories take the vehicle very close to venus's surface indicates that the vehicles direction of motion will be changed by an amount greater than that for the previous launch period. This is indeed true for the table shows that the vehicles velocity vector will be deflected approximately 10° more than the changes occuring for the 1965-6 period.

Figure 15 displays the planetary configuration for the 1967 launch period. It shows that excellent communication with the vehicle should be possible (except of course when it passes behind venus) throughout the entire mission. At the venus and mercury encounters the earth's distance should be approximately .29 and 1.3 A.U. respectively. Figure 16 displays part of the hyperbolic trajectory in the vicinity of venus corresponding to the June 19 launch date.

Earth-Venus-Mercury 1969

The third favorable launch period for these advanced trajectories occures during January of 1969. A fine net calculation was found to be sufficient for determining the trajectories having least launch energy for each launch date. These minimum launch energy trajectories appear in Table 7.

TABLE 7

SOME IMPORTANT PROPERTIES OF EARTH-VENUS-MERCURY TRAJECTORIES

1969

LAUNCH DATE	HEV_1	T_{12}	θ_{12}	$\vec{B}\cdot\vec{T}$	$\vec{B}\cdot\vec{R}$	HEV_2	TISI	DOCA	VACA	DA	T_{23}	θ_{23}	HEV_3	TFT
Jan. 3	4.89	204.76	269.87	-12088.	4899.	6.75	2.04	1634.	11.38	57.34	115.	229.67	9.55	319.76
5	4.77	203.16	268.47	-12254.	4637.	6.68	2.06	1612.	11.35	58.07	111.50	220.23	9.82	314.66
7	4.68	201.76	267.39	-12170.	4655.	6.65	2.07	1510.	11.38	58.85	110.42	217.91	9.94	312.18
9	4.59	200.36	266.32	-12069.	4678.	6.62	2.08	1401.	11.42	59.63	109.42	215.79	10.07	309.78
11	4.48	198.76	264.92	-11941.	4872.	6.57	2.09	1302.	11.44	60.58	109.83	217.51	9.86	308.60
13	4.40	197.37	263.85	-11835.	4850.	6.54	2.10	1186.	11.49	61.33	108.57	214.62	10.05	305.93
15	4.30	195.77	262.45	-11533.	5294.	6.50	2.11	1053.	11.54	62.37	112.00	224.89	9.48	307.77
17	4.22	194.37	261.38	-11581.	4947.	6.47	2.11	954.	11.58	62.99	107.36	212.45	10.13	301.73
19	4.13	192.77	259.99	-11455.	5024.	6.46	2.12	845.	11.63	63.84	107.15	212.37	10.08	299.94
21	4.05	191.18	258.59	-11324.	5081.	6.43	2.13	732.	11.68	64.68	106.85	212.02	10.06	298.03
23	3.96	189.38	256.88	-11209.	5226.	6.39	2.14	645	11.71	65.57	107.67	214.64	9.79	279.05
25	3.89	187.78	255.49	-11079.	5228.	6.37	2.15	529.	11.77	66.33	107.01	213.26	9.86	294.79
27	3.82	185.98	253.79	-10960.	5328.	6.34	2.16	439.	11.81	67.13	107.71	215.52	9.66	293.69
29	3.76	184.39	252.40	-10829.	5277.	6.33	2.16	316.	11.89	67.85	106.55	212.71	9.83	290.94
31	3.70	182.59	250.69	-10713.	5314.	6.31	2.16	221.	11.94	68.56	106.70	213.78	9.75	289.28
Feb. 2	3.65	180.79	248.99	-10596.	5325.	6.30	2.17	124.	12.00	69.24	106.61	213.40	9.73	287.40

The advanced trajectories for the 1965-6 period all have Type II earth-venus transfers and Type II venus-mercury transfers. The trajectories for the 1967 period have Type I earth-venus with Type II venus-mercury transfers. The Type I earth-venus trnsfers caused the flight times for the 1967 trajectories to be much shorter than those required for the 1965-6 trajectories. From Table 7 we notice that these trajectories are very similar to those occuring for the 1965-6 period. Both earth-venus and venus-mercury transfers are Type II. It is important to point out that the minimum launch energy trajectories appearing in Table 4 for the 1965-6 period were obtained from only those trajectories of the fine net having distances of closest approach greater than 800 km. This constraint was not applied to the advanced trajectories of the 1969 period. If this constraint were removed the minimum launch energies would not continually decrease like those for the 1969 period. In addition to continually decreasing launch energies we notice that it has continually decreasing distances of closest approach also. Except for one or two cases these minimum launch energy trajectories also maximized the distances of closest approach. This property also occures for many of the launch dates of the 1965-6 trajectories. Strictly speaking this property did not show up for the 1967 period but since the venus intercept dates are so sensitive for this period their launch energies differed from the lowest for each launch date by an extremely small amount.

Figure 17 gives the planetary configuration during the critical phases of these missions. One observes that at the mercury encounter the sun is almost directly between the earth and mercury. This false representation is due to the fact that the figure is only a rough two dimensional approximation of the real situation. However there should be very serious difficulties with radio communication since mercury will be near its superior conjunction and the earth-sun-mercury angle should be about 168 to 172 degrees. Only the largest radio anterras could perhaps cope with this situation.

Planetary Configuration For Earth-Venus-Mercury 1969
(Jan 23 Trajectory)

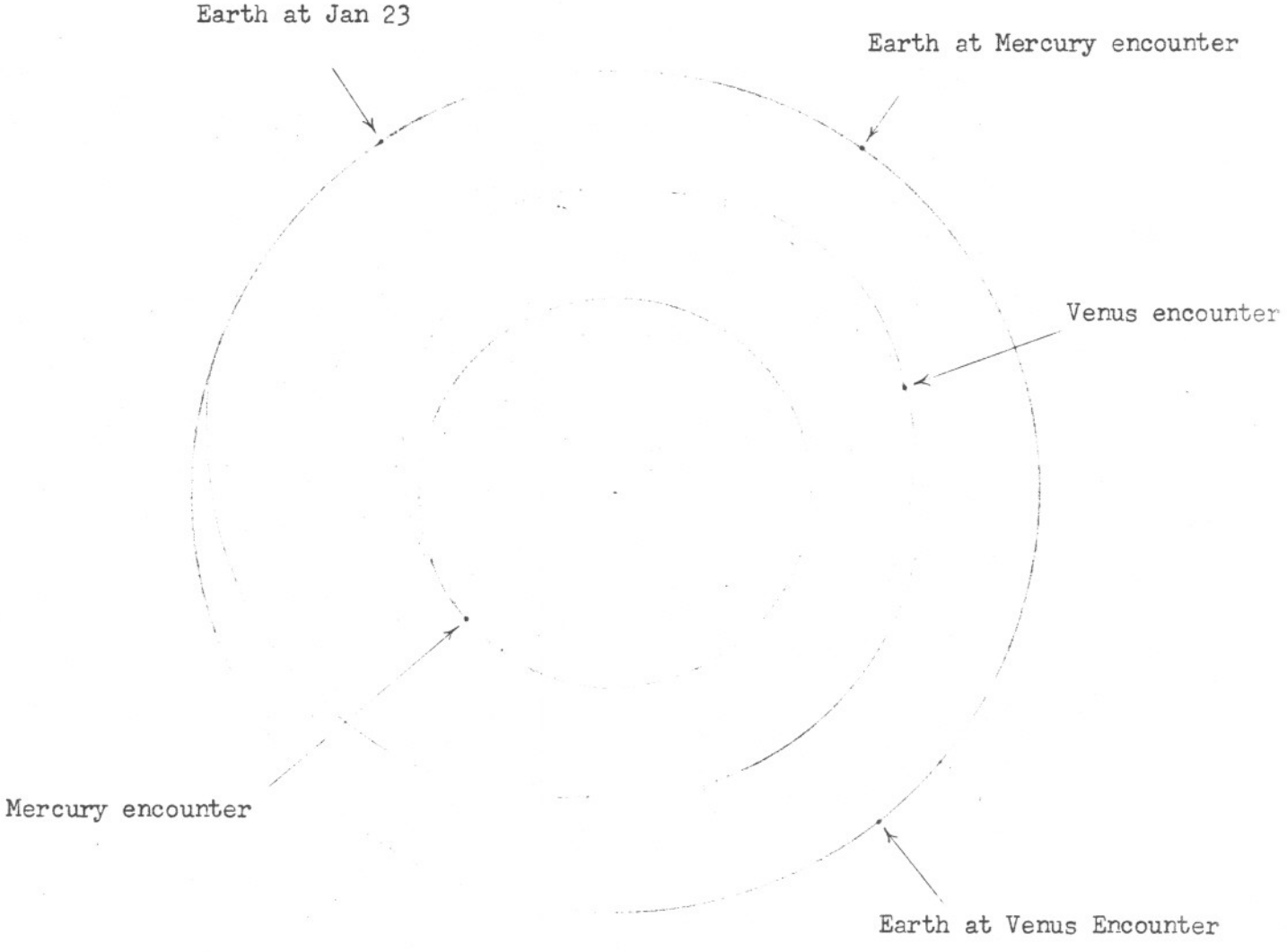

Figure 17

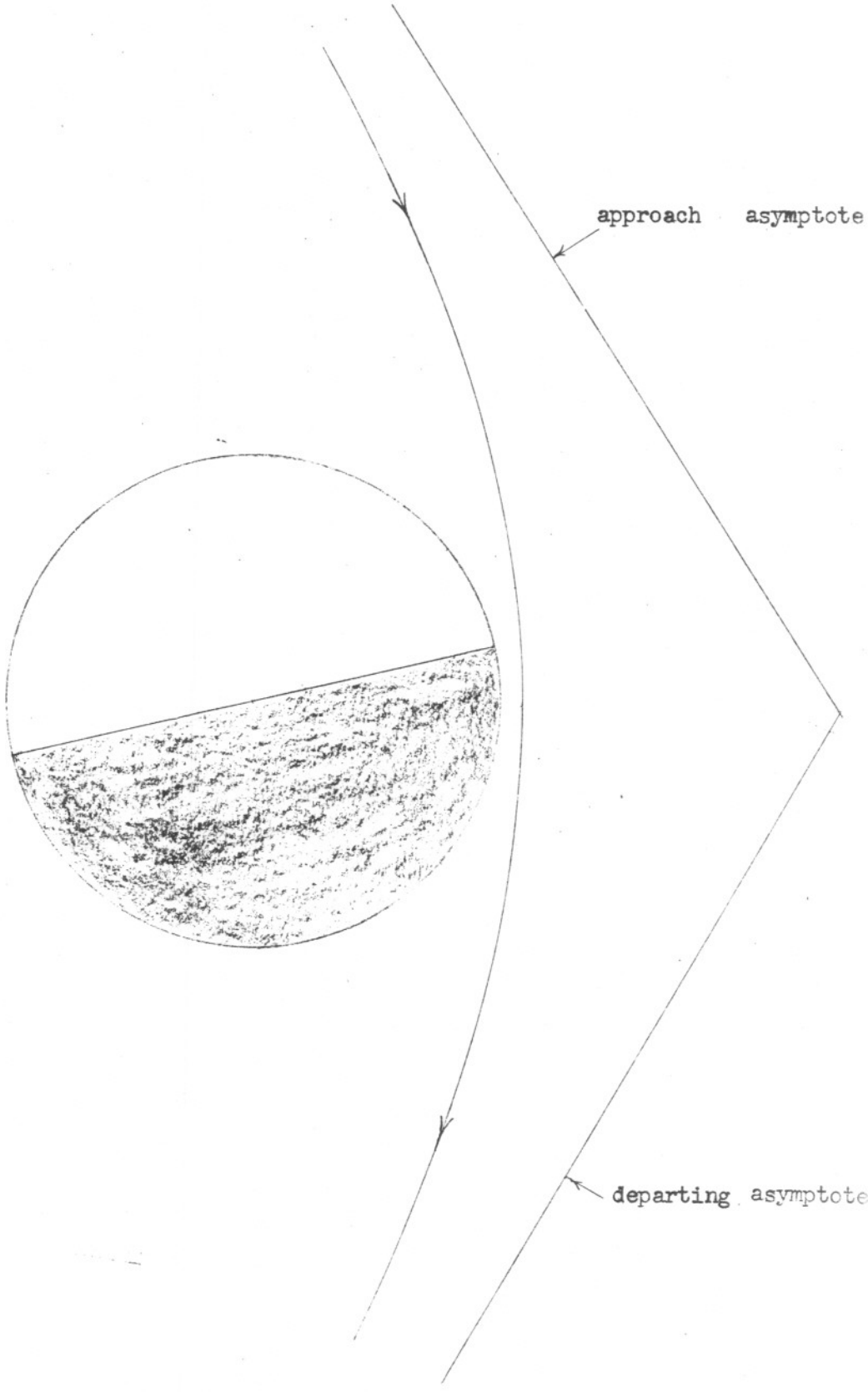

Figure 18

At the venus encounters the communication distances should be approximately 1 A.U. During the mercury encounters the communication distances should be about 1.4 A.U. The January 23 trajectory in the immediate vicinity of venus appears in figure 18.

Earth-Venus-Mercury 1970

The summer of 1970 finds us in the next earth-venus launch period. This period is unusually favorable for this particular type of advanced trajectory. We shall discover later that this launch period is also very favorable for other types of advanced trajectories.

An extra fine net was calculated over this period to find the minimum launch energy trajectories. These trajectories appearing in Table 8 cover a 50 day launch interval. From this table we immediately observe that these trajectories have lower launch energies and shorter flight times than those trajectories of the previous periods. The earth-venus transfers require only about 35% more launch energy than optimum earth-venus trajectories. The short flight times are due to the fact that both earth-venus and venus-mercury transfers are Type I. It must be pointed out however that these trajectories have higher mercury approach energies but by observing the optimum earth-mercury trajectories in Table 2 we find that the approach energies are still much lower than those resulting from the direct flight 1970 trajectories.

The planetary configuration for this launch period is given in figur 19. Notice that the trajectories allow the vehicle to remain relatively near the earth. At the venus encounters the earth is approximately .35 A.U. away. During the mercury encounters the earth is approximately 1.2 A.U. away. The figure shows that these encounters

TABLE 8

EARTH-VENUS-MERCURY

1970

LAUNCH DATE	HEV_1	T_{12}	θ_{12}	$\vec{B}\cdot\vec{T}$	$\vec{B}\cdot\vec{R}$	HEV_2	TISI	DOCA	VACA	DA	T_{23}	θ_{23}	HEV_3	TFT
July 25	3.78	123.23	130.18	13213.	894.	7.07	1.94	2156.	11.34	52.25	58.95	142.67	12.79	182.23
27	3.74	121.46	128.56	13278.	946.	7.12	1.93	2265.	11.33	51.42	58.85	142.62	12.75	180.30
29	3.71	119.64	126.94	13406.	936.	7.16	1.92	2425.	11.29	50.44	58.87	142.97	12.64	178.51
31	3.68	117.82	125.31	13579.	866.	7.21	1.91	2622.	11.24	49.35	59.00	143.63	12.48	176.82
Aug. 2	3.65	115.98	123.67	13607.	949.	7.25	1.90	2698.	11.24	48.71	58.83	143.36	12.49	174.81
4	3.62	114.15	122.02	13727.	924.	7.30	1.88	2850.	11.22	47.83	58.86	143.69	12.39	173.01
6	3.59	112.31	120.37	13895.	829.	7.34	1.87	3040.	11.18	46.84	59.00	144.36	12.25	171.31
8	3.56	110.48	118.72	13996.	808.	7.38	1.86	3173.	11.16	46.06	59.00	144.60	12.18	169.48
10	3.54	108.63	117.04	14090.	785.	7.42	1.85	3300.	11.14	45.33	59.00	144.82	12.12	167.63
12	3.53	106.78	115.37	14181.	758.	7.47	1.85	3423.	11.13	44.62	59.00	145.03	12.06	165.78
14	3.51	104.92	113.68	14163.	893.	7.51	1.84	3454.	11.15	44.20	58.75	144.49	12.10	163.68
16	3.50	103.07	111.99	14112.	1061.	7.55	1.83	3456.	11.18	43.88	58.45	143.77	12.17	161.52
18	3.50	101.22	110.31	14432.	649.	7.59	1.82	3768.	11.11	42.66	59.00	145.66	11.91	160.22
20	3.50	99.35	108.60	14256.	1028.	7.63	1.81	3662.	11.17	42.66	58.41	144.07	12.07	157.76
22	3.51	97.49	106.89	14281.	1064.	7.67	1.80	3725.	11.16	42.19	58.31	143.94	12.06	155.79
24	3.53	95.63	105.19	14630.	504.	7.70	1.79	4056.	11.10	40.99	59.00	146.23	11.78	154.63
26	3.56	93.69	103.36	13413.	2002.	7.76	1.78	3099.	11.44	43.41	56.40	138.33	12.90	150.09
28	3.59	91.89	101.75	14480.	900.	7.78	1.77	4004.	11.17	40.58	58.36	144.67	11.90	150.25
30	3.63	90.02	100.03	14755.	320.	7.82	1.77	4272.	11.12	39.60	59.00	146.77	11.68	149.02
Sept 1	3.68	88.14	98.30	14777.	250.	7.85	1.76	4325.	11.14	39.21	59.00	146.95	11.65	147.14
3	3.75	86.27	96.56	14501.	867.	7.89	1.75	4121.	11.22	39.49	58.18	144.67	11.83	144.45
5	3.82	84.39	94.81	14428.	958.	7.93	1.74	4089.	11.25	39.31	57.98	144.22	11.86	142.37
7	3.91	82.52	93.08	14484.	777.	7.97	1.74	4163.	11.26	38.87	58.13	144.84	11.78	140.64
9	4.02	80.64	91.33	14384.	866.	8.00	1.73	4106.	11.30	38.77	57.91	144.38	11.80	138.55
11	4.14	78.76	89.59	14400.	683.	8.04	1.72	4142.	11.32	38.43	58.05	144.95	11.73	136.81
13	4.27	76.89	87.84	14254.	799.	8.08	1.71	4042.	11.37	38.44	57.79	144.34	11.77	134.67

Planetary Configuration For Earth-Venus-Mercury 1970
(Aug 18 Trajectory)

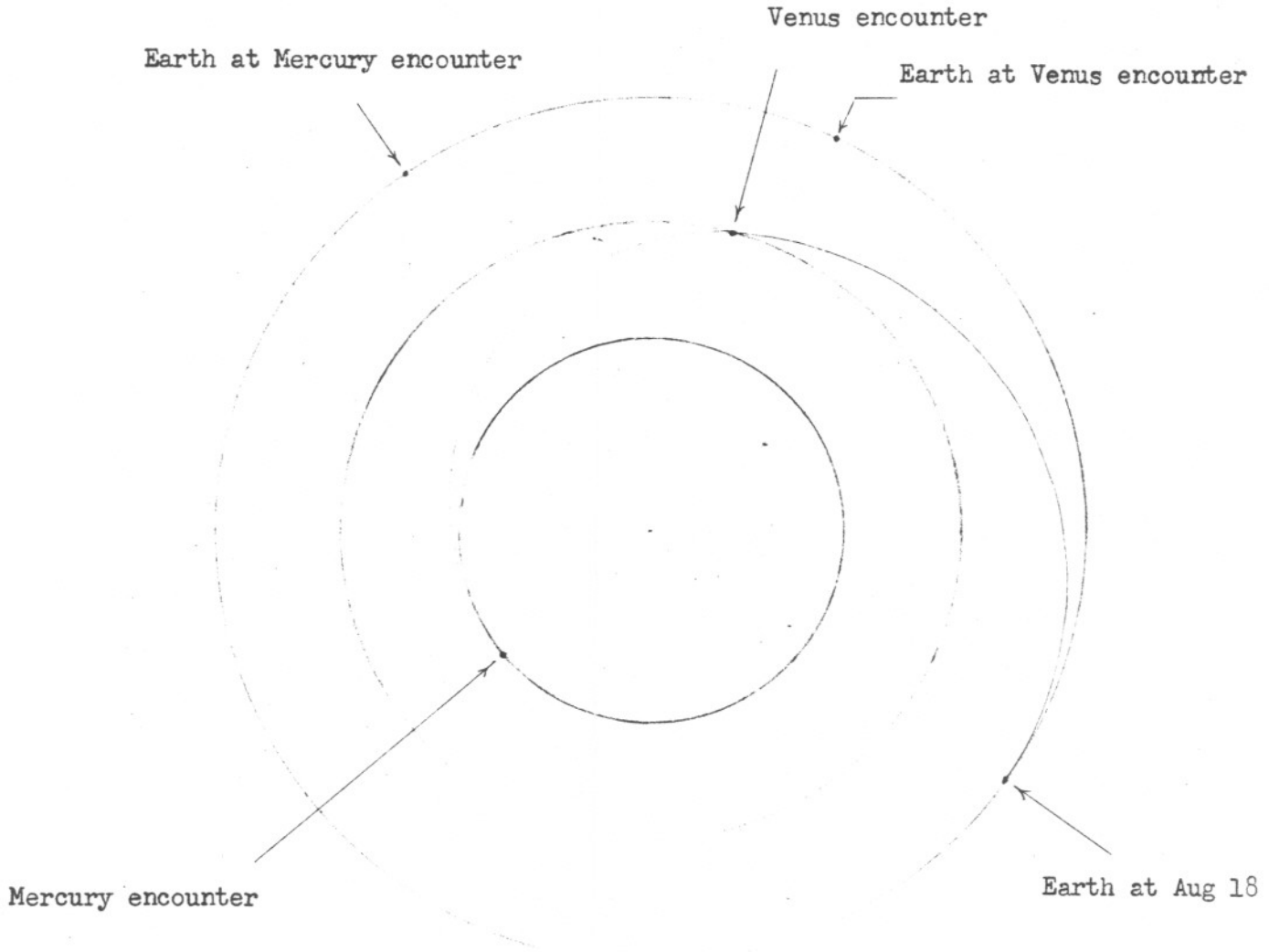

Figure 19

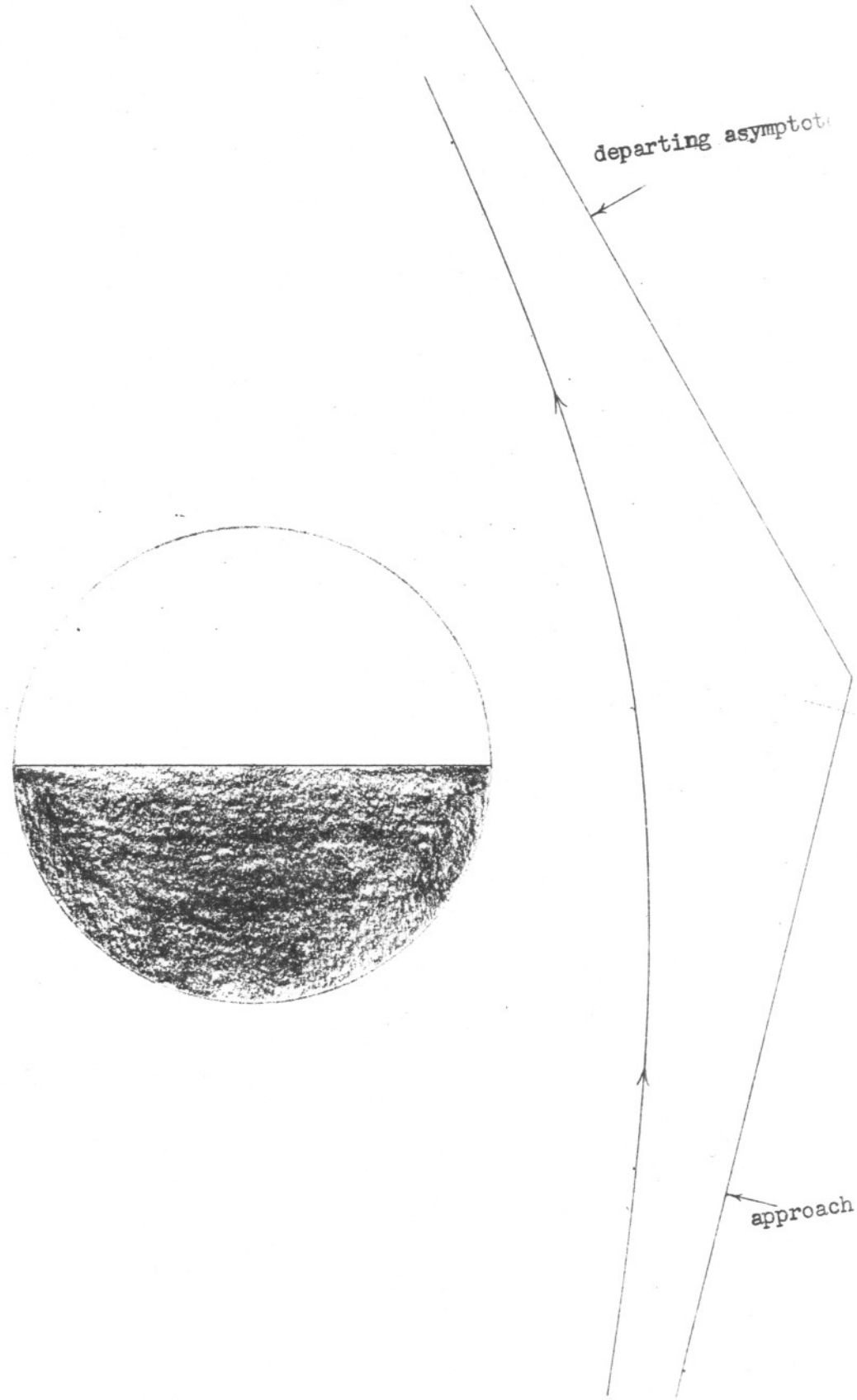

Figure 20

occure when mercury is near greatest elongation. Thus ideal radio communication with the vehicle should be available during these encounters. Figure 20 displays the August 18 trajectory when the vehicle is well within the gravitational sphere of influence of venus. We recall that the radius of this sphere of influence according to the scale of the figure would have a radius of approximately 13 feet.

Earth-Venus-Mercury 1972

The fifth earth-venus launch period occures during the spring of 1972. The advanced trajectories of this period will take a vehicle fairly close to venus's cloud layer. An extra fine net was calculated so that the trajectories having maximum closest approach distance could be found. These trajectories which are given in Table 9 also minimize the launch energy. This property which appeared in the first 3 launch periods was absent from the 1970 trajectories.

The earth-venus and venus-mercury transfers are Type II and Type I respectively and hence are very similar to those corresponding to the 1969 period. Both periods have continually decreasing launch energies.

From Table 2 one observes that this is the first period which has mercury approach energies higher than those resulting from the optimum direct earth-mercury trajectories. This undesirable property cannot be removed by sacrificing a little launch energy because any change would require closer distance of closest approach.

Figure 21 shows the planetary configuration for this launch period. The venus and mercury encounters occure approximately 1.2 and 1.4 A.U. from the earth respectively.

The trajectory close to venus having the April 1 launch date appears in Figure 22.

TABLE 9

EARTH-VENUS-MERCURY

1972

LAUNCH DATE	HEV_1	T_{12}	θ_{12}	$\vec{B}\cdot\vec{T}$	$\vec{B}\cdot\vec{R}$	HEV_2	TINS	DOCA	VACA	DA	T_{23}	θ_{23}	HEV_3	TFT
March 18	4.62	206.70	272.60	-10283.	-3956.	7.61	1.81	654.	12.41	53.97	87.28	153.53	15.22	293.98
20	4.52	205.15	271.34	-10685.	-2830.	7.54	1.82	630.	12.38	54.66	85.51	149.16	15.86	290.66
22	4.43	203.72	270.27	-10716.	-2797.	7.49	1.83	610.	12.37	55.15	85.00	148.40	15.84	288.72
24	4.33	202.21	269.08	-10717.	-3105.	7.44	1.85	637.	12.32	55.50	85.00	148.97	15.56	287.21
26	4.25	200.80	268.06	-10495.	-3914.	7.40	1.85	643.	12.29	55.81	85.58	151.25	14.97	286.38
28	4.19	199.60	267.37	-10142.	-4506.	7.39	1.86	545.	12.34	56.36	85.76	152.66	14.55	285.36
30	4.10	198.00	266.05	-10272.	-4401.	7.33	1.87	563.	12.30	56.78	85.29	151.82	14.55	283.29
April 1	4.03	196.58	265.01	-10211.	-4501.	7.30	1.88	521.	12.30	57.27	85.00	151.67	14.40	281.58
3	3.94	194.97	263.67	-10789.	-2648.	7.25	1.89	432.	12.33	58.18	82.00	143.85	15.78	276.97
5	3.86	193.32	262.27	-10818.	-2864.	7.20	1.90	458.	12.28	58.52	82.00	144.27	15.56	275.32
7	3.78	191.70	260.91	-10827.	-3082.	7.15	1.91	474.	12.25	58.87	81.99	144.67	15.34	273.69
9	3.71	190.05	259.51	-10821.	-3302.	7.11	1.92	483.	12.21	59.23	82.00	145.10	15.13	272.05
11	3.65	188.41	258.13	-10794.	-3521.	7.07	1.93	481.	12.19	59.61	82.00	145.52	14.93	270.41
13	3.59	186.77	256.77	-10747.	-3738.	7.03	1.94	470.	12.18	59.98	82.00	145.93	14.73	268.77
15	3.54	185.13	255.39	-10681.	-3950.	7.00	1.95	449.	12.17	60.39	82.00	146.34	14.54	267.13
17	3.50	183.50	254.02	-10595.	-4157.	6.97	1.96	417.	12.18	60.81	82.00	146.75	14.35	265.50
19	3.46	181.94	252.80	-10447.	-4384.	6.96	1.96	359.	12.21	61.26	82.00	147.24	14.12	263.94
21	3.44	180.34	251.49	-10298.	-4593.	6.94	1.97	296.	12.24	61.74	82.00	147.69	13.94	262.34

Planetary Configuration For Earth-Venus-Mercury 1972

(April 1 Trajectory)

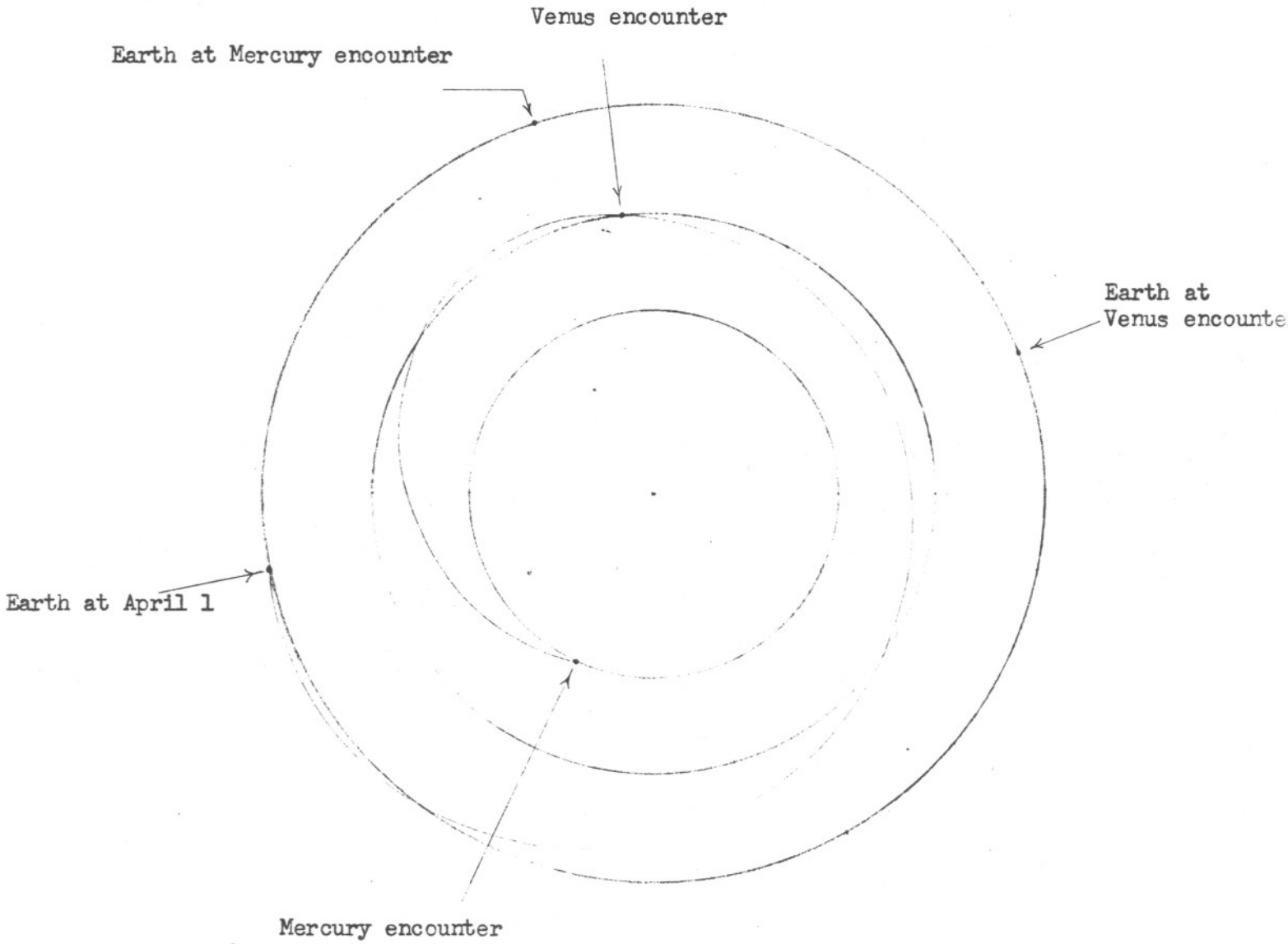

Figure 21

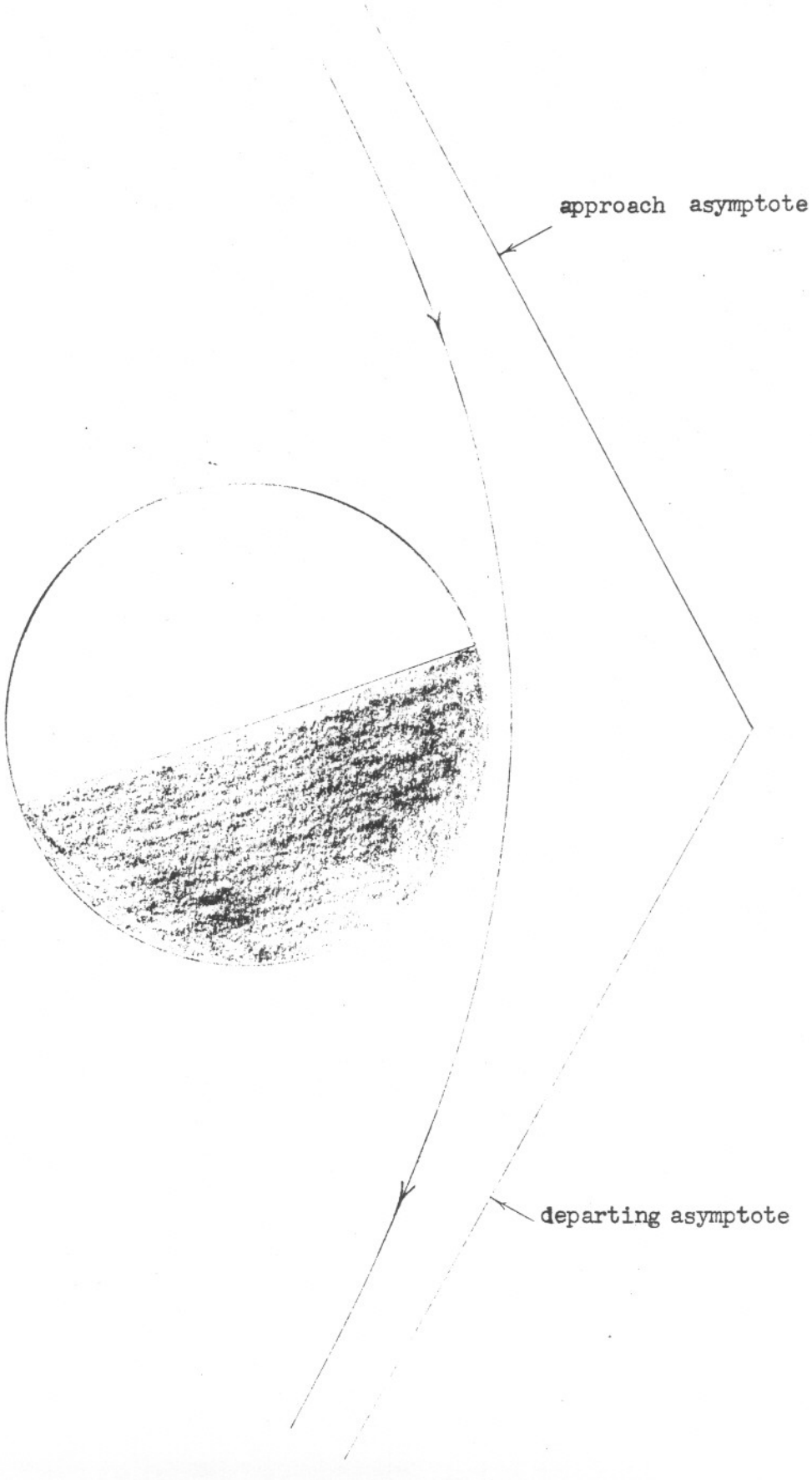

Figure 22

Earth-Venus-Mercury 1973

The last launch period for the decade occures during the winter of 1973. The advanced trajectories of this period do not require very close approaches although the launch energies were found to be fairly high. Consequently an extra fine net was calculated and the resulting minimum launch energy trajectories appear in Table 10. These trajectories have Type I earth-venus and venus-mercury transfers yielding very short total flight times. Consequently these trajectories closely resemble those of the 1970 period. It is interesting to note however that for the 1970 period one finds low launch energies but high mercury approach energies while for the 1973 trajectories these characteristics are reversed. The distances of closest approach are neither maximum nor minimum.

The planetary configuration for this launch period appears in figure 23. The earth's distance at the venus and mercury encounters is approximately .32 and 1.2 A.U.'s respectively.

The trajectory corresponding to the November 4 launch date near venus appears in figur 24.

b. Earth-Venus-Mars Trajectories

The method of calculating nets employed for the numerical analysis of the earth-venus-mercury trajectories were used for all the advanced trajectories considered in this paper. Thus for the earth-venus-mars trajectories which we now consider, six coarse nets with grid 6 by 6 were calculated about the six earth-venus launch periods appearing in Table 1. These preliminary calculations showed that three of these periods required relatively long flight times and hence were discarded. The three remaining were the 1968-9, 1970 and the 1972 periods. Since the sophisticated vehicles required for these advanced trajectories will probably not be available before 1968, these three periods should be idealy suited to the time interval when they could be effectively utilized.

TABLE 10

EARTH-VENUS-MERCURY

1973

LAUNCH DATE	HEV_1	T_{12}	θ_{12}	$\vec{B}\cdot\vec{T}$	$\vec{B}\cdot\vec{R}$	HEV_2	TISI	DOCA	VACA	DA	T_{23}	θ_{23}	HEV_3	TFT
Oct. 21	4.39	106.56	115.30	12558.	-5758.	7.86	1.75	3423.	11.40	41.68	58.00	136.29	10.86	164.56
23	4.36	104.73	113.58	12706.	-5800.	7.89	1.75	3596.	11.37	40.92	57.59	135.32	10.81	162.32
25	4.33	102.91	111.88	12342.	-6008.	7.93	1.74	3400.	11.46	41.26	57.87	136.35	10.90	160.78
27	4.30	101.09	110.19	12078.	-6160.	7.96	1.73	3271.	11.52	41.40	58.00	136.94	10.97	159.09
29	4.28	99.26	108.47	11997.	-6259.	8.00	1.72	3275.	11.54	41.14	57.88	136.83	10.99	157.15
31	4.26	97.44	106.76	11733.	-6383.	8.03	1.72	3139.	11.61	41.31	58.00	137.38	11.06	155.44
Nov. 2	4.25	95.61	105.04	11610.	-6474.	8.07	1.71	3107.	11.65	41.17	57.93	137.39	11.08	153.54
4	4.25	93.79	103.34	11370.	-6567.	8.10	1.70	2983.	11.71	41.31	58.00	137.83	11.14	151.79
6	4.25	91.97	101.61	11228.	-6643.	8.13	1.70	2931.	11.75	41.23	57.94	137.88	11.17	149.91
8	4.25	90.14	99.89	10992.	-6712.	8.17	1.69	2802.	11.82	41.40	58.00	138.27	11.23	148.14
10	4.27	88.31	98.16	10933.	-6770.	8.20	1.68	2810.	11.84	41.13	57.82	137.98	11.23	146.14
12	4.29	86.49	96.45	10601.	-6814.	8.24	1.68	2594.	11.94	41.59	58.00	138.72	11.33	144.49
14	4.33	84.66	94.71	10450.	-6852.	8.27	1.67	2521.	11.99	41.59	57.94	138.76	11.36	142.60
16	4.37	82.83	92.98	10365.	-6887.	8.31	1.66	2499.	12.02	41.42	57.78	138.52	11.36	140.61

Planetary Configuration For Earth-Venus-Mercury 1973
(Nov 4 Trajectory)

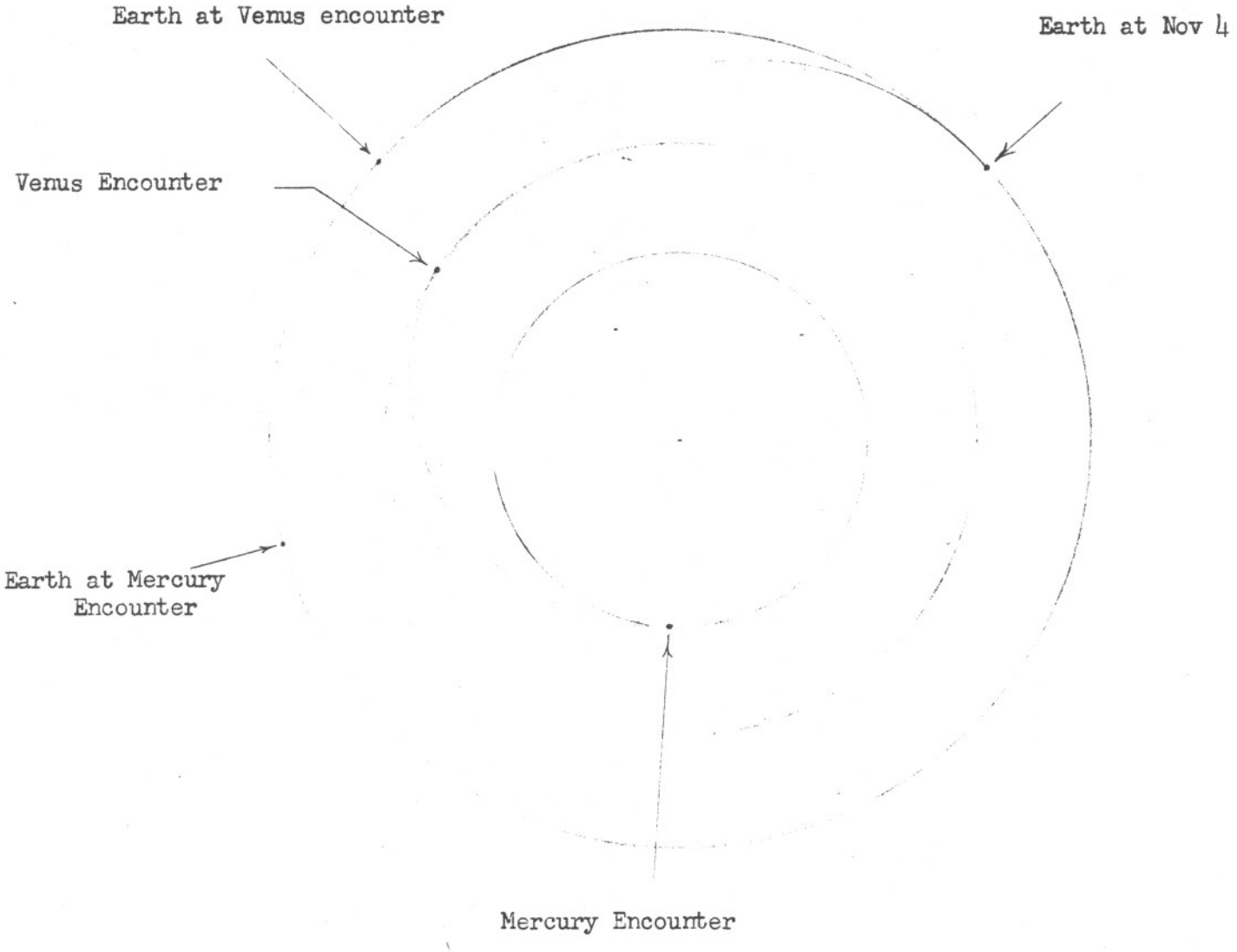

Figure 23

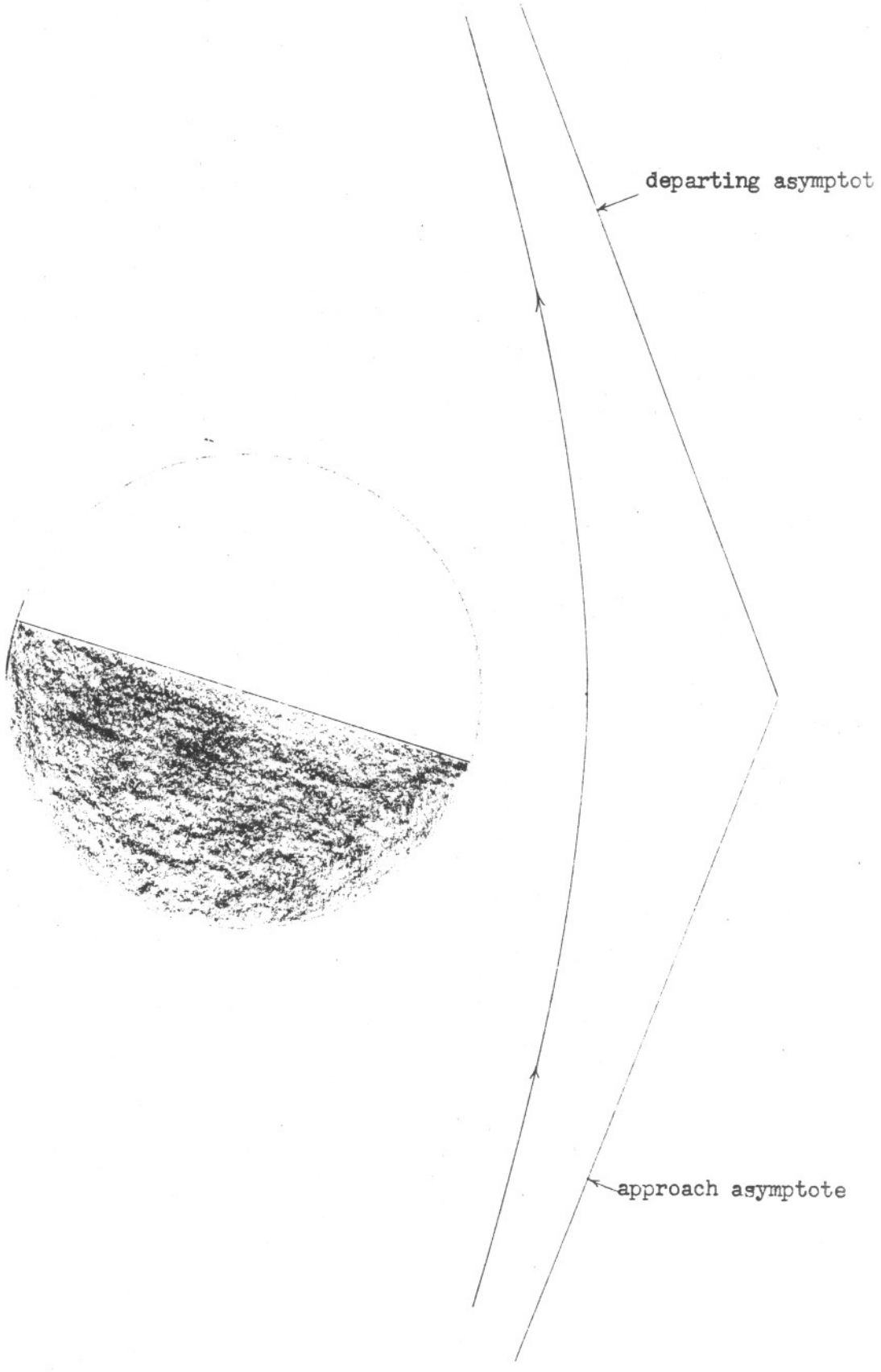

Figure 24